2. THERMOCHRONOLOGIC CONSTRAINTS FOR THE TECTONIC EVOLUTION OF THE MORESBY SEAMOUNT, WOODLARK BASIN, PAPUA NEW GUINEA[1]

Brian D. Monteleone,[2] Suzanne L. Baldwin,[2] Trevor R. Ireland,[3] and Paul G. Fitzgerald[2]

ABSTRACT

During Ocean Drilling Program (ODP) Leg 180, 11 sites were drilled in the vicinity of the Moresby Seamount to study processes associated with the transition from continental rifting to seafloor spreading in the Woodlark Basin. This paper presents thermochronologic (^{40}Ar/^{39}Ar, ^{238}U/^{206}Pb, and fission track) results from igneous rocks recovered during ODP Leg 180 that help constrain the latest Cretaceous to present-day tectonic development of the Woodlark Basin.

Igneous rocks recovered (primarily from Sites 1109, 1114, 1117, and 1118) consist of predominantly diabase and metadiabase, with minor basalt and gabbro. Zircon ion microprobe analyses gave a ^{238}U/^{206}Pb age of 66.4 ± 1.5 Ma, interpreted to date crystallization of the diabase. ^{40}Ar/^{39}Ar plagioclase apparent ages vary considerably according to the degree to which the diabase was altered subsequent to crystallization. The least altered sample (from Site 1109) yielded a plagioclase isochron age of 58.9 ± 5.8 Ma, interpreted to represent cooling following intrusion. The most altered sample (from Site 1117) yielded an isochron age of 31.0 ± 0.9 Ma, interpreted to represent a maximum age for the timing of subsequent hydrothermal alteration. The diabase has not been thermally affected by Miocene–Pliocene rift-related events, supporting our inference that these rocks have remained at shallow and cool levels in the crust (i.e., upper plate) since they were partially reset as a result of middle Oligocene hydrothermal alteration. These results suggest that

[2]Department of Geosciences, PO Box 210077, University of Arizona, Tucson AZ 85721, USA. Present address: Department of Earth Sciences, Syracuse University, Syracuse NY 13244-1070, USA. Correspondence author: **sbaldwin@syr.edu**
[3]Department of Earth and Planetary Sciences, Stanford University, Stanford CA 94305, USA. Present address: Research School of Earth Sciences, The Australian National University, Canberra ACT 0200, Australia.

B.D. Monteleone et al.
Thermochronologic Constraints for Tectonic Evolution

2

crustal extension in the vicinity of the Moresby Seamount, immediately west of the active seafloor spreading tip, is being accommodated by normal faulting within latest Cretaceous to early Paleocene oceanic crust.

Felsic clasts provide additional evidence for middle Miocene and Pliocene magmatic events in the region. Two rhyolitic clasts (from Sites 1110 and 1111) gave zircon ^{238}U/^{206}Pb ages of 15.7 ± 0.4 Ma and provide evidence for Miocene volcanism in the region. ^{40}Ar/^{39}Ar total fusion ages on single grains of K-feldspar from these clasts yielded younger apparent ages of 12.5 ± 0.2 and 14.4 ± 0.6 Ma due to variable sericitization of K-feldspar phenocrysts.

^{238}U/^{206}Pb zircon, ^{40}Ar/^{39}Ar K-feldspar and biotite total fusion, and apatite fission track analysis of a microgranite clast (from Site 1108) provide evidence for the existence of a rapidly cooled 3.0- to 1.8-Ma granitic protolith. The clast may have been transported longitudinally from the west (e.g., from the D'Entrecasteaux Islands). Alternatively, it may have been derived from a more proximal, but presently unknown, source in the vicinity of the Moresby Seamount.

INTRODUCTION

Active continental rifting, metamorphic core complex development, and seafloor spreading makes the western Woodlark Basin of Papua New Guinea an ideal area to study processes associated with the initial rupture of continental lithosphere (e.g., Hill et al., 1995; Taylor et al., 1999, and references therein). Ocean Drilling Program (ODP) Leg 180 was designed to examine processes associated with continental rifting, including low angle normal faulting, sedimentary basin evolution, and the movement of footwall blocks during the final stages of rifting and prior to seafloor spreading initiation (Taylor, Huchon, Klaus, et al, 1999).

One of the objectives of ODP Leg 180 was to determine the pressure-temperature-time (P-T-t) history of recovered igneous and metamorphic rocks to constrain the tectonic evolution of the Moresby Seamount, a bathymetric high bounded on its northern flank by a seismically active low-angle normal fault (Abers et al., 1997). The north-south transect drilled just west of the spreading tip recovered diabase, gabbro, basalt, and sedimentary rocks. We present results of a thermochronologic study of diabase and felsic igneous clasts recovered from sites drilled on the hanging wall and footwall of the normal fault bounding the Moresby Seamount. Results allow us to constrain, in part, the prerifting tectonic evolution of the region and the geologic setting prior to the onset of crustal extension and seafloor spreading in the vicinity of the Moresby Seamount. Results are interpreted in the context of the present-day tectonic setting and the geologic evolution of the Papuan Peninsula.

PRESENT-DAY TECTONIC SETTING

The Woodlark Basin is located in the Solomon Sea southeast of Papua New Guinea (Fig. F1). The present-day tectonics of the region are the result of interactions between microplates caught in and formed during oblique convergence between the Pacific and Indo-Australian plates (Benes et al., 1994; Tregoning et al., 1998). Counterclockwise rotation

F1. Present-day tectonic setting of eastern Papua New Guinea and the Solomon Islands, p. 18.
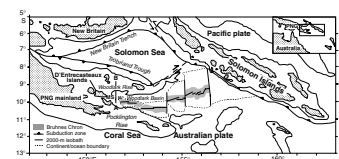
of the Solomon microplate within this plate boundary zone led to the development of an oceanic spreading center. Magnetic anomalies indicate that the seafloor spreading center has propagated westward into eastern Papua New Guinea since at least 6 Ma (Weissel et al., 1982; Benes et al., 1994; Taylor et al., 1995, 1999; Goodliffe et al., 1997). Progressive opening of the western Woodlark Basin due to seafloor spreading led to separation of the formerly contiguous crust of the Pocklington and Woodlark Rises. The seafloor spreading tip is currently located at 9.8°S, 151.7°E. West of the seafloor spreading center, continental extension is manifested by full and half grabens, active metamorphic core complexes, and rift-related peralkaline volcanism (e.g., Smith and Simpson, 1972; Davies, 1973; Smith, 1976; Hegner and Smith, 1992; Davies and Warren, 1988; Hill et al., 1992, 1995; Hill and Baldwin, 1993; Baldwin et al., 1993; Stolz et al., 1993; Hill, 1994).

The Moresby Seamount is a bathymetric high located ~20–30 km west of the spreading tip and east of the D'Entrecasteaux Islands active metamorphic core complexes. Earthquake and seismic reflection data indicate that the seamount is bounded on its northern side by a seismically active, low-angle normal fault that strikes east-west and dips 25°–30° toward the north (Abers et al., 1997; Taylor, Huchon, Klaus, et al., 1999). The location of the fault within kilometers of the spreading tip allows for continental extension to be studied just prior to the transition to seafloor spreading.

LEG 180 DRILLING RESULTS

An extensive description of Leg 180 drilling results can be found in the Leg 180 *Initial Reports* volume (Taylor, Huchon, Klaus, et al., 1999) and in this volume. Eleven sites were drilled on both the footwall and hanging wall of the active low-angle normal fault (Fig. F2). Rocks recovered from the northern hanging wall sites revealed the presence of a complete mid-Pliocene to Holocene rift-basin sedimentary sequence overlying a unit of basalt and diabase rocks at Sites 1109 and 1118 and unconformably overlying an inferred Miocene forearc basin conglomerate at Site 1115 (Robertson et al., in press). Drilling of the southern footwall recovered lesser amounts of rift subsidence-related sediments overlying diabase rocks at Site 1114 and diabase grading to gabbro at Site 1117. The first few meters of coring at Site 1117 also recovered fault gouge interpreted to be related to recent normal faulting (Taylor, Huchon, Klaus, et al., 1999).

Most igneous rocks recovered from the footwall (Sites 1114 and 1117) and at the base of the hanging wall rift-basin strata (Sites 1109 and 1118) were cored as a mafic sequence consisting of a thin layer of basaltic clasts overlying several meters of diabase, which increased in grain size to gabbro at deeper levels (Site 1117). The rocks were variably altered and brecciated, with greenschist-grade metamorphism, hydrothermal alteration, brecciation, and deformation decreasing with depth away from the fault surface in the footwall sites. These rocks were cored from the footwall (i.e., Sites 1114 and 1117 on the Moresby Seamount) directly beneath the fault and from within a conglomerate below middle- to late-Pliocene rift-basin strata in the hanging wall (Site 1118) and as far north as the southern Trobriand Platform (Site 1109). Diabase clasts from Sites 1109 and 1118 above the low-angle normal fault are rounded and have "onion skin" oxidation rinds consistent with subaerial fluvial deposition (Robertson et al., in press). Formation Micro-

F2. Bathymetry and structures near Moresby seamount and lithostratigraphy of Sites 1108–1116, p. 19.
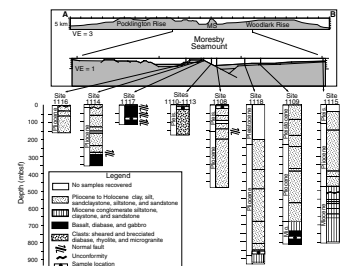
Scanner (FMS) log imaging and rounded diabase clasts recovered from the hanging wall at Site 1118 indicate the presence of a diabase boulder conglomerate with clast sizes ranging from 5 cm to ~2–3 m (Taylor, Huchon, Klaus, et al., 1999).

Igneous and metamorphic rocks from Site 1114 were cored at the top of the Moresby Seamount below 286 m of Pliocene–Pleistocene claystone, siltstone, and sandstone and consist of diabase and lower greenschist facies metadiabase. Sixty-seven meters of rock was recovered; the majority was brecciated and variably hydrothermally altered and metamorphosed. Hydrothermal alteration is inferred by the presence of secondary quartz and epidote veins, both containing disseminated pyrite. Original diabase mineralogy includes equal amounts of plagioclase and clinopyroxene with accessory magnetite. Secondary phases include quartz, calcite, epidote, and chlorite. Rocks at Site 1114 are the most altered and brecciated among the sites containing igneous and metamorphic rocks.

Quartz gabbro was cored from greater structural depth within the Moresby Seamount (relative to Site 1114) and directly beneath the low-angle normal fault zone at Site 1117. The first 1.5 m recovered from Hole 1117A consisted of light green fault-gouge material containing talc, chlorite, calcite, ankerite, and three forms of serpentine: chrysotile, lizardite, and antigorite. Quartz gabbro cored below the fault zone is the most likely protolith for the gouge material, as talc, chlorite, and serpentine are common alteration products of mafic and ultramafic rocks. Mylonitic epidote and chlorite-rich rocks were cored directly beneath the gouge, giving way to diabase breccia and undeformed quartz gabbro with depth. Bands of sheared epidote- and chlorite-rich rocks exist below the fault-gouge material. They are interpreted to be related to the fault zone directly above, but the timing and depth at which shearing occurred is unknown. Undeformed gabbro at Site 1117 has a similar modal mineralogy to diabase from Site 1114 and has patchy hydrothermal alteration with secondary mineralization similar to that of diabase from Site 1114.

Basalt and diabase were cored at Sites 1109 and 1118 at 740 and 860 mbsf, respectively, below a mid-Pliocene to Holocene sequence of sediments and sedimentary rocks interpreted to have formed during rifting and subsidence (Taylor, Huchon, Klaus, et al., 1999). The uppermost part of the mafic unit is a calcite-cemented basaltic conglomerate containing ≤10-cm-diameter clasts, grading with depth to a diabase conglomerate. Although the mafic rocks recovered comprise a conglomerate unit in the uppermost parts of each site, it is not certain that the lowermost parts of the units are in place or part of the same conglomerate unit. Large intact cores recovered deeper within the units represent either large boulders within a conglomerate or in situ mafic rocks. However, FMS imaging strongly suggests that the lowermost portion of the mafic rocks cored at Site 1118 are indeed part of a large boulder conglomerate (Taylor, Huchon, Klaus, et al., 1999). Diabase from Sites 1109 and 1118 has modal mineralogy similar to samples from Sites 1114 and 1117, but the intensity of hydrothermal alteration varies from site to site. Site 1109 diabase is the least altered of the four sites and contains equal amounts of mostly pristine plagioclase and clinopyroxene with both ophitic and granular textures. Site 1118 is extensively hydrothermally altered and contains saussuritized plagioclase and veins of quartz, calcite, pyrite, and chlorite.

A larger diversity of rock types, including a microgranite and hydrothermally altered felsic volcanics, mica schists, carbonate schists, and

B.D. Monteleone et al.
Thermochronologic Constraints for Tectonic Evolution

5

highly sheared mafic rocks, was cored at the top of the hanging wall sedimentary strata close to the Moresby Seamount at Sites 1108 and 1110–1113. Robertson et al. (in press) interpreted these clasts as detritus resulting from Pleistocene initiation and movement of the low-angle normal fault, depositing larger, angular clasts on top of deep-water sediments that were deposited during regional rift-related subsidence. However, longitudinal transport and deposition of at least some of these clasts from nearby sources (e.g., the D'Entrecasteaux Islands to the west) cannot be ruled out, because lithologies other than diabase and gabbro were not cored in place in the vicinity of the Moresby Seamount.

ANALYTICAL PROCEDURES

$^{40}Ar/^{39}Ar$ total fusion and step heating experiments, $^{238}U/^{206}Pb$ ion microprobe analyses, and apatite fission track dating were undertaken on selected samples of igneous rocks recovered during Leg 180 to document their temperature-time history. Table T1 summarizes the samples analyzed in this study.

$^{40}Ar/^{39}Ar$ Analyses

$^{40}Ar/^{39}Ar$ analyses were conducted on plagioclase and clinopyroxene separates from two diabase samples from Sites 1109 and 1118 on the hanging wall and one gabbro sample from Site 1117 on the footwall. $^{40}Ar/^{39}Ar$ total fusion and step heat experiments were also conducted on single crystals of K-feldspar from two small rhyolite clasts from Sites 1110 and 1111. $^{40}Ar/^{39}Ar$ total fusion analyses were conducted on feldspar and biotite from a microgranite recovered at Site 1108.

High-purity mineral separates (>99%) were prepared from crushed and sized rock chips using conventional heavy liquid and magnetic separation techniques. Mineral separates were wrapped individually in Sn foil along with biotite standard GA1550 (97.9 Ma) used to monitor the neutron dose (McDougall and Harrison, 1999). Samples were vacuum sealed in super-silica quartz tubes and irradiated for 5 hr in position L-67 of the Ford reactor at the University of Michigan.

Argon analyses were performed in the noble gas laboratory at the University of Arizona. Extraction of gas from the samples was accomplished using a double-vacuum, resistance-heated tantalum furnace with temperature control via a thermocouple in contact with the bottom of the crucible and mounted on the outer (low) vacuum side of the furnace. Three SAES getters were used for purification of the extracted gas. Isotopic analyses were performed using a VG5400 mass spectrometer with an ion-counting electron multiplier. Machine mass discrimination and sensitivity were determined from repeated analysis of atmospheric argon. Data reduction was completed using in-house programs. Samples were corrected for blanks, neutron-induced interfering isotopes, decay of ^{37}Ar and ^{39}Ar, mass discrimination, and atmospheric argon, as well as $H^{35}Cl$, $H^{36}Cl$, and $H^{37}Cl$. Correction factors used to account for interfering nuclear reactions were determined by analyzing argon extracted from irradiated CaF_2 and K_2SO_4. All ages are calculated using the decay constants recommended by Steiger and Jäger (1977). Stated precisions for $^{40}Ar/^{39}Ar$ ages include all uncertainties in the measurement of isotopic ratios and are quoted at the 1-σ level. The errors do not include an error associated with the J parameter, which is <0.5%.

U/Pb Analyses

Zircon U/Pb ages were determined using the Stanford University sensitive high-resolution ion microprobe (SHRIMP RG). Zircon separates were prepared from clasts of microgranite (<75 μm) (Core 180-1108B-6R) and rhyolite (<106 μm) (Cores 180-1110B-3X and 180-1111A-16R) using conventional heavy liquid and magnetic separation techniques. Zircons were mounted in epoxy along with 1099-Ma standard AS57 from the Duluth anorthosite complex (Paçes and Miller, 1989). The mount was polished to expose midsections. Cathodoluminescence images were obtained to aid in spot location. Zircons from diabase Core 180-1117A-11R were analyzed in situ in thin section. These zircons were typically 10–15 μm in maximum dimension. Standards were analyzed from the second mount held in the source chamber and were interspersed with the in situ Core 180-1117A-11R analyses.

The operating conditions and techniques for the SHRIMP RG are similar to those described by Muir et al. (1996). Analyses were performed using a 6- to 7-nA primary O^- beam focused to a ~25-μm elliptical spot. A mass resolution of 7,000 M/ΔM (full width; 10% maximum) was used to eliminate isobaric interferences. $^{206}Pb^+/U^+$ ratios were normalized against UO^+/U^+ and then calibrated against the AS57 standard. U and Th concentrations were normalized to the ANU SL13 standard (U = 238 ppm and Th = 20 ppm; ±20% variation). Common Pb was monitored with ^{204}Pb, but $^{204}Pb/^{206}Pb$ is an insensitive monitor of common Pb in the young zircons analyzed. Ages were determined from the $^{206}Pb/^{238}U$ ratio at the concordia from an extrapolation through common Pb and the individual data points (^{207}Pb correction). Thus, data on the Tera-Wasserburg plots use uncorrected Pb isotopic compositions. Common Pb, as determined from the $^{207}Pb/^{206}Pb$ ratio, was low in the epoxy mounts and substantially higher in the thin section. The relatively high common Pb in thin section is probably a result of cracks and grain boundaries containing common Pb rather than being intrinsic to the zircon. Nevertheless, data from all samples provided well constrained ages.

Fission Track Analysis

To constrain the lower-temperature thermal history of these samples, we attempted to separate out apatite for fission track analysis. Unfortunately, the lithologies recovered are mostly unfavorable for the presence of apatite and we only found apatite in datable quantities in the microgranite clast (Core 180-1108B-6R). Samples were prepared for fission track analysis using standard procedures (Fitzgerald et al., 1999).

RESULTS AND INTERPRETATIONS

Basalt, Diabase, and Gabbro

X-Ray Fluorescence Data

X-ray fluorescence (XRF) analyses conducted on board the *JOIDES Resolution* show that diabase and gabbro from footwall sites (1114 and 1117) and hanging wall sites (1109 and 1118) are chemically similar, varying only in K, Ba, Rb, and Sr (Taylor, Huchon, Klaus, et al., 1999). Movement of these mobile elements is likely associated with hydrother-

mal alteration, which is further supported by the presence of epidote and pyrite within veins of heavily altered samples. In addition, the abundance of these mobile elements increases as a function of the degree of alteration within the samples, as determined by thin section analysis and loss-on-ignition values, which tend to increase with increasing alteration. These data suggest, at least on a first-order basis, that mafic rocks from the various hanging wall and footwall sites are variably altered but petrogenetically related.
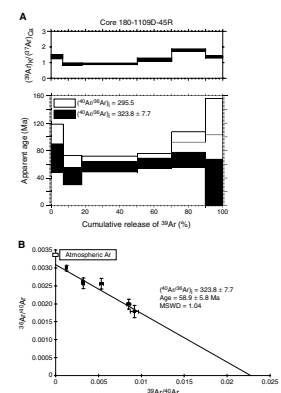
^{40}Ar/^{39}Ar Results

^{40}Ar/^{39}Ar analyses of diabase and gabbro samples were challenging because of the low K content within the plagioclase and pyroxene separates. An average of ~0.001%–0.006% K within the grains at all sites (Monteleone, 2000) rendered both total fusion and step heating experiments on clinopyroxene unsuccessful. As such, ^{40}Ar/^{39}Ar dating of clinopyroxene provided no interpretable results.

Although shipboard XRF analyses suggest that the diabase and gabbro rocks are petrogenetically related and vary only in amount of hydrothermal alteration, total fusion ages of plagioclase separates from Sites 1109, 1117, and 1118 are strikingly discordant and imprecise (Tables T1, T2). This apparent contradiction can be resolved by comparing ^{40}Ar/^{39}Ar apparent ages and variation of $(^{40}$Ar/^{36}Ar$)_i$ (the ratio of the initial nonradiogenic Ar component) as revealed on an isochron diagram along with assessment of K alteration of plagioclase grains within each sample. Potassium alteration, observed in XRF whole-rock analyses, is also observed in plagioclase grains within the samples. Results from four selected diabase/gabbro samples from Cores 180-1109D-45R, 180-1117A-11R, 180-1117-alt, and 180-1118A-70R, indicate variable $(^{40}$Ar/^{36}Ar$)_i$ ratios and a younging of ^{40}Ar/^{39}Ar apparent ages with increasing K alteration. Two end-member apparent ages can be identified and are interpreted to date plagioclase cooling and a younger K alteration event as discussed below.

Ophitic diabase from Site 1109 was shown to be the least altered by XRF and microprobe analyses (Monteleone, 2000). Diabase from Core 180-1109D-45R consists of ~50% plagioclase, ~50% clinopyroxene, and <1% pyrite, magnetite, and ilmenite as accessory phases. Microprobe point analyses and transects of plagioclase indicate percent K variations from 0.014 to 0.038 across individual grains (Monteleone, 2000). The ^{40}Ar/^{39}Ar step heat experiment yielded a saddle-shaped age spectrum with an imprecise minimum apparent age of 60.5 ± 10.7 Ma (Fig. F3). The analyses reveal a nonradiogenic trapped argon composition $(^{40}$Ar/^{36}Ar$)_i$ of 323.8 ± 7.7, which is higher than the atmospheric ratio (295.5) and indicates the presence of either inherited or excess ^{40}Ar within the plagioclase grains. Figure F3 shows the corrected ^{40}Ar/^{39}Ar spectrum assuming an atmospheric $(^{40}$Ar/^{36}Ar$)_i$ and the ^{40}Ar/^{39}Ar age spectrum assuming a $(^{40}$Ar/^{36}Ar$)_i$ of 323.8 ± 7.7, derived from a best-fit line from an isochron diagram. A plot of $(^{39}$Ar$)_K$/$(^{37}$Ar$)_{Ca}$, proportional to the K/Ca ratio, shows little variation between steps, with a range of values from 1–2.5. Given the complex form of the spectrum, the isochron age of 58.9 ± 5.8 Ma is interpreted as the best estimate for the age of this plagioclase sample and we interpret the data to represent the timing of cooling following crystallization. The relatively large error is due to the low K content of the sample.

T2. ^{40}Ar/^{39}Ar analytical results, p. 30.

F3. ^{40}Ar/^{39}Ar age spectrum and $(^{39}$Ar$)_K$/$(^{37}$Ar$)_{Ca}$ and isochron plots for Core 180-1109D-45R, p. 20.

B.D. Monteleone et al.
Thermochronologic Constraints for Tectonic Evolution

8

Diabase Core 180-1118A-70R is the most altered of the selected samples, containing equal amounts of plagioclase and clinopyroxene, with extensive chlorite alteration, accessory pyrite, ilmenite, titanite, and magnetite (Fig. F4). Pyroxene grains contain ~0.001% K, similar to those from Core 180-1109D-45R, but plagioclase is extensively altered. Microprobe point analyses show a random variation of K content within plagioclase grains, with K ranging from 0.01% (as in unaltered Core 180-1109-45R) to ~6.5% K in areas of abundant alteration (Monteleone, 2000). $^{40}Ar/^{39}Ar$ analysis of Core 180-1118A-70R thus provides an estimate for the age of the alteration event. $^{40}Ar/^{39}Ar$ step heat results for this sample yielded a complex spectrum without a well-defined plateau. Although extensively altered, the $(^{40}Ar/^{36}Ar)_i$ is close to atmospheric in composition (300.8 ± 1.8) (Fig. F4). The $(^{39}Ar)_K/(^{37}Ar)_{Ca}$ ratio is variable, ranging from 40 to 200, which is one to two orders of magnitude higher than $(^{39}Ar)_K/(^{37}Ar)_{Ca}$ ratios for unaltered Core 180-1109D-45R. We infer that most of the argon extracted from this sample is due to outgassing of potassic alteration phases (e.g., sericite) within the plagioclase. The isochron age of 31.0 ± 0.9 Ma is interpreted as the maximum age of alteration. The higher K content within the altered plagioclase (Core 180-1118A-70R) allows for higher precision in $^{40}Ar/^{39}Ar$ apparent ages as compared to the low percent K content of unaltered plagioclase from Core 180-1109D-45R.

Ophitic gabbro Core 180-1117A-11R is variably altered, and thus it is difficult to interpret results in the context of a plagioclase cooling age or age of K alteration. The sample has a similar modal mineralogy to those from Sites 1109 and 1118 but with coarser grain size (Fig. F5). Two separates were prepared, each exhibiting different degrees of K alteration within plagioclase grains. These were separated magnetically, based on the assumption that the samples would have varying degrees of magnetic susceptibility as a function of the degree of alteration. Magnetic separation produced white grains (nonmagnetic and less altered) and green grains (magnetic and altered). The less altered plagioclase separate is referred to as Core 180-1117A-11R, and the more altered separate is referred to as Core 180-1117-alt. Microprobe analysis reveals that alteration is variable between individual plagioclase grains of Core 180-1117A-11R, with overall K alteration intermediate between pristine plagioclase of Core 180-1109D-45R and extensively altered Core 180-1118A-70R (Monteleone, 2000). A $^{40}Ar/^{39}Ar$ step heat experiment on Core 180-1117A-11R (less altered separate) yielded a saddle-shaped age spectrum (Fig. F5; Table T2). On an isochron plot, the data reveal an age of 43.6 ± 2.5 Ma, with a corresponding $(^{40}Ar/^{36}Ar)_i$ of 355.4 ± 4.2. Although the isochron age cannot be related to a specific tectonic event, as expected given its moderate degree of K alteration, it is intermediate in age between isochron ages for unaltered Core 180-1109D-45R (58.9 ± 7.7 Ma) and pervasively altered Core 180-1118A-70R (31.0 ± 0.9 Ma). It likely reflects the outgassing of a mixture of unaltered plagioclase grains and moderately altered plagioclase grains. The $(^{39}Ar)_K/(^{37}Ar)_{Ca}$ is variable and higher than corresponding $(^{39}Ar)_K/(^{37}Ar)_{Ca}$ ratios for unaltered Core 180-1109D-45R.

Core 180-1117-alt also yielded a complex age spectrum (Fig. F6; Table T2). The data plotted on an isochron plot yield an age of 35.4 ± 1.0 Ma, which corresponds to a $(^{40}Ar/^{36}Ar)_i$ of 392.3 ± 8.7. The isochron age for Core 180-1117-alt is slightly older than the isochron age obtained on the most altered sample (Core 180-1118A-70R) (31.0 ± 0.9 Ma).
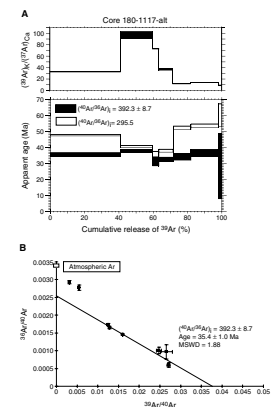
F4. $^{40}Ar/^{39}Ar$ age spectrum and $(^{39}Ar)_K/(^{37}Ar)_{Ca}$ and isochron plots for Core 180-1118A-70R, p. 21.
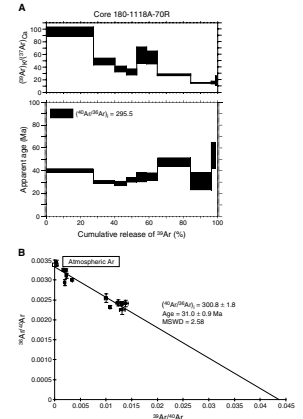
F5. $^{40}Ar/^{39}Ar$ age spectrum and $(^{39}Ar)_K/(^{37}Ar)_{Ca}$ and isochron plots for Core 180-1117A-11R, p. 22.
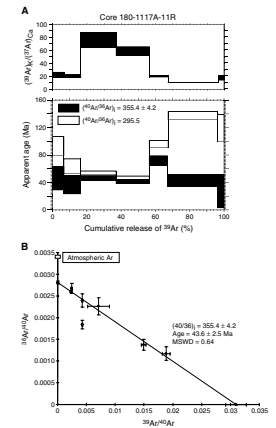
F6. $^{40}Ar/^{39}Ar$ age spectrum and $(^{39}Ar)_K/(^{37}Ar)_{Ca}$ and isochron plots for Core 180-1117-alt, p. 23.

U/Pb Results

A number of zircons were identified in diabase Core 180-1117A-11R, although many were too small for analysis. Seven analyses of zircon are presented in Table T3 and on a Tera-Wasserburg plot in Figure F7. These zircons show very high trace element concentrations with a range in U concentrations from 656 to 7609 ppm, Th from 2099 ppm to near 3 wt%, and Th/U from 1.93 to 6.95. U-Pb ages from these zircons are more scattered than would be predicted from a single population dispersing between radiogenic and common Pb end-members. Five of the seven analyses lie within the error of a best-fit line, indicating an age of 66.4 ± 1.5 Ma (2 σ_m; mean squared weighted deviates [MSWD] = 1.55). Of the other two analyses, number 6.1 is slightly lower than the mean but has a large error. Analysis number 5.1, on the other hand, at 75.6 ± 3.6 Ma (2 σ), is significantly older than the other analyses and their mean. It is unlikely that this age represents inheritance in the diabase. Rather, this age is symptomatic of an artifact of the U-Pb calibration in the presence of extreme U and Th concentrations. In this case, the Th for this analysis represents nearly 3 wt%, whereas all but number 6.1, which shows the low age, are <1 wt%. For this reason, both analyses 5.1 and 6.1 have been excluded. The remaining data lie within error of each other, despite a range in Th concentration from 2000 to 9000 ppm. The correlation between high U-Pb age and abnormally high U or Th concentrations is likely a result of enhanced Pb+ production, relative to U+, from a matrix with elevated mean density. Such observations are not unusual in secondary ion mass spectrometry, where ion production can be strongly influenced by matrix parameters. The $^{238}U/^{206}Pb$ zircon age of 66.4 ± 1.5 Ma for diabase from Hole 1117A is interpreted as the age of crystallization.

Clasts

Small (2–5 cm) igneous and metamorphic clasts were recovered from the top of Pliocene to Holocene synrift sedimentary sections at Site 1108 and in Holes 1110B and 1111A; several were selected for thermochronologic analysis. The clasts are angular, and their size suggests a proximal source.

Rhyolite Clasts

$^{40}Ar/^{39}Ar$ Results

Two K-feldspar-phyric rhyolite clasts sampled from Holes 1110B and 1111A contain 1–5 mm moderately sericitized K-feldspar grains within a felsic groundmass. Electron microprobe analyses indicated that the groundmass chemistry for these clasts is similar (Monteleone, 2000), suggesting that the clasts are petrogenetically related, although K-feldspar grains are variably altered to sericite. $^{40}Ar/^{39}Ar$ total fusion ages from K-feldspar grains from these samples yield ages of 12.5 ± 0.3 and 14.4 ± 0.6 Ma (Table T2) for Cores 180-1110B-3X and 180-1111A-16R, respectively, suggesting that K alteration may have partially reset the $^{40}Ar/^{39}Ar$ apparent ages in both samples. $^{40}Ar/^{39}Ar$ step heat analyses produce disturbed spectra that can be interpreted to reflect the effects of partial resetting of argon systematics as the result of a subsequent thermal event, slow cooling, and/or hydrothermal alteration (Figs. F8, F9). Preserved volcanic textures and the presence of sericite alteration
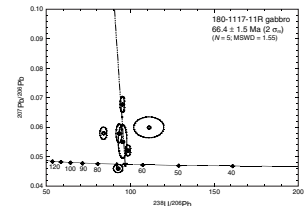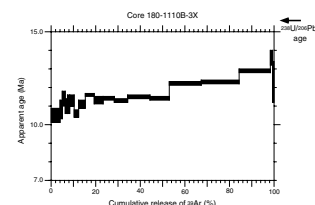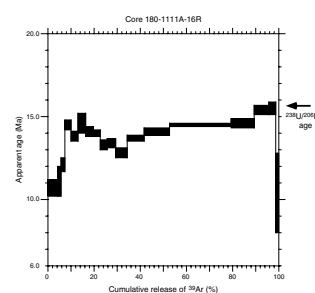
within K-feldspar grains makes low-temperature hydrothermal alteration the most likely cause of resetting of argon systematics. Integrated $^{40}Ar/^{39}Ar$ apparent ages from Cores 180-1110B-3X and 180-1111A-16R are 11.9 ± 0.2 and 14.1 ± 0.3 Ma, respectively. These are concordant with total fusion ages on the same samples (Table T2). The highest temperature step of Core 180-1111A-16R K-feldspar is concordant with the $^{238}U/^{206}Pb$ age of 15.7 ± 0.3 Ma (see below), suggesting that sericite may not have affected the argon systematics within the most retentive sites within the phenocryst. The lowest temperature step for each sample gave an apparent age between 10 and 11 Ma, which we interpret is the result of hydrothermal alteration subsequent to eruption.

U/Pb Results

Rhyolite from Sites 1110 and 1111 were considered together because of the similarities in the zircons and results. The zircons are typically tabular, 50–100 μm long, and have aspect ratios of ~3:1–5:1. U-Th-Pb data are presented in Table T3; a Tera-Wasserburg plot is shown in Figure F10. The zircons show a range in U concentrations from 74 to 465 ppm (on average higher in Site 1111) and Th concentrations from 1 to 130 ppm. The Th/U ratios are typically <0.1 (13 of 16 analyses); of the remaining three analyses, one analysis is of an inherited core. This inherited core has a U-Pb age of 96 ± 6 Ma (2 σ), indicating the presence of Cretaceous crust in the area during the formation of the rhyolites. The remaining analyses all lie within error of a mixing line between radiogenic Pb at 15.7 ± 0.4 Ma (2 σ_m; MSWD = 0.44) and common Pb of the same age (Cumming and Richards, 1975). Thus, the K-feldspar-phyric rhyolite clasts cored near (and possibly deposited from) the Moresby Seamount are interpreted to be petrogenetically related, crystallized at 15.7 ± 0.4 Ma, and variably hydrothermally altered at 10–11 Ma.

F10. Tera-Wasserburg plot of zircons, p. 27.

Granite Clast

Core 180-1108B-6R contains a ~3-cm microgranite clast deposited in the Pleistocene and recovered from the top of synrift oceanic sediments. The sample contains ~70% albite, ~15% microcline, ~10% quartz, and 5% biotite, chlorite, and amphibole. Accessory phases include pyrite, apatite, zircon, and sphene. $^{40}Ar/^{39}Ar$ total fusion ages from biotite and "feldspar" (a mixture of albite and microcline) are 2.6 ± 0.4 and 2.2 ± 0.6 Ma, respectively (Table T2). Apatite fission track dating gave an age of 2.7 ± 1.2 Ma (2 σ) (Table T4). Apatite fission track dating was difficult because of the poor quality of apatite crystals and low spontaneous track density. However, the fission track age is within the error limits of the more precise $^{40}Ar/^{39}Ar$ total fusion ages for biotite and feldspar.

T4. Apatite fission track analytical results, p. 34.

Only two zircons were identified from microgranite from Site 1108. They were small (<50 μm) and equant. One grain is 550 Ma and has 116 ppm U and 78 ppm Th, whereas a young grain at 3.1 ± 0.1 Ma has 1448 ppm U and 664 ppm Th. The common Pb content of the young grain is quite low, with a measured $^{207}Pb/^{206}Pb$ of 0.072 being close to the radiogenic end-member, and, therefore, the age is rather insensitive to the common Pb composition used. This grain may therefore represent the magmatic age, although a single analysis is not statistically reliable on its own. However, the close similarity to the range in $^{40}Ar/^{39}Ar$ total fusion ages does lend support to this interpretation. These data suggest

B.D. Monteleone et al.
Thermochronologic Constraints for Tectonic Evolution

11
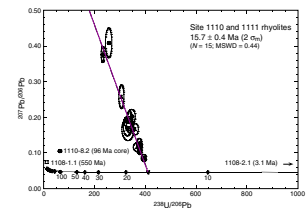
that the microgranite crystallized at 3.1 Ma, rapidly cooled by ~2.6 Ma, and we infer it was shallowly emplaced.

DISCUSSION

Davies' (1980b) model for the tectonic assembly of Papua New Guinea calls for pre-Eocene northeastward subduction of the Australian plate beneath the Pacific plate, creating an island arc. This collision resulted in underthrusting and metamorphism of Australian plate continental rocks along with southward obduction of oceanic crust and mantle from the Pacific plate (Davies, 1980a). Subduction polarity reversed to southwestward subduction following Eocene collision (Cooper and Taylor, 1987), creating the Trobriand Trough and a volcanic arc above an ophiolitic basement, which overlies metamorphosed Paleocene arc and subducted Australian crustal rocks. In eastern Papua New Guinea, Paleogene arc convergence, continent/arc collision, and ophiolite emplacement preceded continental rifting and the transition to oceanic crustal development and growth (Davies and Smith, 1971; Davies 1973, 1980b; Weissel et al., 1982; Baldwin et al., 1993; Benes et al., 1994).

The presence of ubiquitous basalt, diabase, and gabbro with grain size increasing with depth suggests that the Moresby Seamount may be comprised, at least in part, of oceanic crust (Taylor, Huchon, Klaus, et al., 1999). Sedimentary evidence for subaerial deposition of diabase conglomerate places these rocks above sea level prior to regional rift-related subsidence. Thermochronologic results from this study indicate that diabase and gabbro recovered during ODP Leg 180 did not form as a result of Pliocene–Holocene seafloor spreading in the western Woodlark Basin but instead likely represents latest Cretaceous–early Paleocene oceanic crust. Furthermore, the diabase recovered during Leg 180 has not been thermally affected by Miocene–Pliocene rift-related events. We infer that these rocks have remained at shallow and cool levels in the crust (i.e., upper plate) since they were partially reset as a result of middle Oligocene hydrothermal alteration.

It is tempting to correlate the basalt, diabase, and gabbro recovered during Leg 180 with rocks of the Papuan Ultramafic Belt (PUB) of southeast Papua New Guinea. The PUB is believed to represent oceanic crust and upper mantle obducted over the Australian continental lithosphere during arc-continent collision (Davies, 1980b). K-Ar ages on gabbroic and basaltic portions of the PUB are 147–150 and 116 Ma, respectively (Davies and Smith, 1971; Davies 1980b). Although interpretation of this data is problematic, these K-Ar ages are considerably older than the zircon $^{238}U/^{206}Pb$ age (66.4 ± 1.5 Ma) interpreted to date crystallization of the diabase recovered during Leg 180. In the Musa-Kumusi divide of Papua New Guinea, 66- to 56-Ma K-Ar and $^{40}Ar/^{39}Ar$ hornblende ages from granulites from the sole of the PUB have been interpreted to date the emplacement of the PUB (Lus et al., 1998). These data suggest the PUB represents Late Jurassic to Early Cretaceous(?) oceanic crust that was emplaced in the Paleocene.

ODP Leg 180 basalt, gabbro, and diabase may be related to tholeiitic lavas and boninite lavas from the Dabi Volcanics on the Papuan Peninsula, which have $^{40}Ar/^{39}Ar$ total fusion and plateau ages of 58.9 ± 1.1 and 58.8 ± 0.8 Ma, respectively (Walker and McDougall, 1982). These data are concordant with the $^{40}Ar/^{39}Ar$ isochron age on plagioclase from the least-altered diabase (from Site 1109). Furthermore, Leg 180 basalt,

gabbro, and diabase may be petrogenetically related to undated gabbro and ultramafic rocks exposed in the D'Entrecasteaux Islands (Davies, 1973), where they occur in the upper plate of active metamorphic core complexes (Hill et al., 1992).

Diabase and gabbro recovered during Leg 180 are petrologically and chemically similar between sites with respect to mineralogy, texture, and nonmobile major and trace elements but are heterogeneous with respect to degree of alteration and incorporation of "excess" or inherited ^{40}Ar. Hydrothermal alteration has had a drastic effect on the resetting of argon systematics within these rocks. A correlation clearly exists involving increasing hydrothermal alteration within plagioclase grains and decreasing apparent $^{40}Ar/^{39}Ar$ ages (Fig. F11). $^{40}Ar/^{39}Ar$ isochron ages constrain the age for plagioclase cooling at 58.9 ± 5.8 Ma for unaltered Core 180-1109D-45R and provide a maximum age of K alteration of 31.0 ± 0.9 Ma for pervasively altered Core 180-1118A-70R.

Plagioclase step heat experiments for all analyzed samples revealed nonatmospheric $(^{40}Ar/^{36}Ar)_i$ ratios indicative of incorporation of excess argon. Although the mechanism for incorporation of excess argon is not completely understood, it is commonly observed in plagioclase, as has been demonstrated in this and many other studies (cf. Harrison and McDougall, 1981; Pringle, 1993; Claesson and Roddick, 1983). Empirical evidence suggests that argon retentivity in plagioclase is somewhat lower than for biotite (McDougall and Harrison, 1999). Thus, the plagioclase isochron age for the least altered sample (Core 180-1109D-45R) provides evidence that the diabase cooled to temperatures below ~200°–250°C by ~59 Ma.

Rhyolite and microgranite clasts analyzed from Sites 1108, 1110, and 1111 were most likely derived from the vicinity of the Moresby Seamount. These clasts record two tectonic events related to prerift volcanism and synrift magmatism. Zircons from rhyolites with a $^{238}U/^{206}Pb$ age of 15.7 ± 0.3 Ma provide evidence for mid-Miocene volcanic activity in the region. One zircon had an inherited 96 ± 6 Ma (2 σ) core, indicating the presence of Cretaceous crust in the area during the formation of the rhyolites. The rhyolites were subsequently hydrothermally altered at 10–11 Ma, perhaps as the result of subsequent magmatic activity. Ash fall tuff layers from Site 1115 have similar $^{40}Ar/^{39}Ar$ apparent ages of 13.8 and 14.0 Ma (Lackshewitz et al., 2001). The tuffs are present in the Miocene section below an unconformity, which has been interpreted to represent the transition from subduction and forearc development to rift-related regional subsidence. Thus, protoliths for volcanic clasts from Holes 1110B and 1111A most likely formed during a period of Miocene arc magmatism. Additional evidence for magmatism at this time is found in the Milne Basic Complex on the Papuan Peninsula where 12- to 16-Ma felsic rocks intrude the undated Milne Basic Complex (Smith, 1982).

Although no in situ continental basement was recovered during Leg 180, the ~3-cm-diameter microgranite clast from Site 1108 (Core 180-1108B-6R) provides at present the only evidence for a granitic protolith in the vicinity of the Moresby Seamount that can be temporally related to rift-related magmatism in the western Woodlark Basin. Its small grain size and late Pliocene $^{238}U/^{206}Pb$ zircon, $^{40}Ar/^{39}Ar$ biotite and feldspar, and apatite fission track ages suggest that the microgranite was emplaced at shallow (i.e., cool) levels of the Earth's crust. The protolith for this clast crystallized at 3.0 Ma, cooled rapidly by ~2.2 Ma, and was subsequently eroded, transported, and deposited as a clast meters above
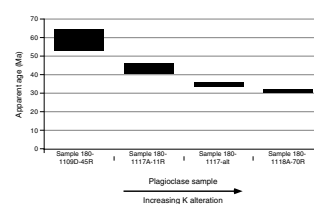
the northern bounding normal fault of the Moresby Seamount. Similar granitic protoliths exist in the D'Entrecasteaux Islands (Baldwin et al., 1993), suggesting that the clast may have been transported longitudinally from the west. Alternatively, it may have been derived from a more proximal, but presently unknown, source in the vicinity of the Moresby Seamount.

Although the Moresby Seamount is a crustal block bounded on its northern flank by a seismically active low-angle normal fault (Abers, 1991) in an area of continental extension just west of the active seafloor spreading tip, it does not possess many of the features characteristic of metamorphic core complexes (cf. Crittenden et al., 1980; Coney and Harms, 1984). Leg 180 did not recover in situ crustal rocks exhumed from great depths as is the case for lower plate rocks of the D'Entrecasteaux Islands to the west (Baldwin et al., 1993). However, the diabase and gabbro recovered during Leg 180 may possibly have correlations with undated ultramafic and mafic rocks found in the upper plate above detachment faults on the D'Entrecasteaux Islands. Active crustal extension in the vicinity of the Moresby Seamount is being accommodated by normal faulting within latest Cretaceous to early Paleocene oceanic crust.

CONCLUSIONS

Thermochronologic data for diabase recovered during Leg 180 indicates that the diabase crystallized at 66.4 Ma. Although highly heterogeneous in terms of K alteration and $(^{40}Ar/^{36}Ar)_i$, $^{40}Ar/^{39}Ar$ step heat experiments on plagioclase from diabase and gabbro from the Moresby Seamount yielded an age of 58.9 ± 5.8 Ma for the least altered sample (Core 180-1109D-45R); the data are interpreted to represent cooling following crystallization. A $^{40}Ar/^{39}Ar$ isochron age for highly altered plagioclase from diabase Core 180-1118A-70R provides an estimate of the age of subsequent hydrothermal alteration at 31.0 ± 0.9 Ma. The diabase has not been thermally affected by Miocene–Pliocene rift-related events, supporting our inference that these rocks have remained at shallow (i.e., cool) depths in the crust since they were partially reset as a result of middle Oligocene hydrothermal alteration. Although the relationship of Leg 180 diabases with those from eastern PNG is not firmly established, a reexamination of similar mafic rocks from the Papuan Ultramafic Belt and the Milne Basic Complex is required in light of the results presented here. This, along with further geochemical comparisons, will establish more firmly the nature and timing of the tectonic evolution of the Papuan Peninsula.

$^{40}Ar/^{39}Ar$ and $^{238}U/^{206}Pb$ dating of rhyolite clasts (Cores 180-1110B-3X and 180-1111A-16R) derived from the vicinity of the Moresby Seamount provide evidence for volcanic activity at 15.7 ± 0.3 Ma followed by hydrothermal alteration at 10–11 Ma. These ages are interpreted to reflect arc magmatism possibly related to subduction at the Trobriand Trough. A microgranite clast (Core 180-1108B-6R) provides evidence for synrift felsic magmatism, as the clast was derived from a rapidly cooled, shallowly emplaced 3.0-Ma protolith in the vicinity of the Moresby Seamount.

ACKNOWLEDGMENTS

REFERENCES

Abers, G.A., 1991. Possible seismogenic shallow-dipping normal faults in the Wood-lark-D'Entrecasteaux extensional province, Papua New Guinea. *Geology,* 19:1205–1208.

Abers, G.A., Mutter, C.Z., and Fang, J., 1997. Shallow dips of normal faults during rapid extension: earthquakes in the Woodlark-D'Entrecasteaux rift system, Papua New Guinea. *J. Geophys. Res.,* 102:15301–15317.

Baldwin, S.L., Lister, G.S., Hill, E.J., Foster, D.A., and McDougall, I., 1993. Thermo-chronologic constraints on the tectonic evolution of active metamorphic core complexes, D'Entrecasteaux Islands, Papua New Guinea. *Tectonics,* 12:611–628.

Benes, V., Scott, S.D., and Binns, R.A., 1994. Tectonics of rift propagation into a conti-nental margin: western Woodlark Basin, Papua New Guinea. *J. Geophys. Res.,* 99:4439–4455.

Claesson, S., and Roddick, J.C., 1983. ^{40}Ar/^{39}Ar data on the age and metamorphism of the Ottfjallet diabases, Sarv Nappe, Swedish Caledonides. *Lithos,* 16.

Coney, P.J., and Harms, T.A., 1984. Cordilleran metamorphic core complexes: Ceno-zoic extensional relics of Mesozoic compression, *Geology,* 12:550–554.

Cooper, P., and Taylor, B., 1987. Seismotectonics of New Guinea: a model for arc reversal following arc-continent collision. *Tectonics,* 6:53–67.

Crittenden, M.D., Coney, P.J., and Davis, G.H., 1980. Cordilleran metamorphic core complexes. *Mem. Geol. Soc. Am.,* 153:1–490.

Cumming, G.L., and Richards, J.R., 1975. Ore lead isotope ratios in a continuously changing earth. *Earth Planet. Sci. Lett.,* 28:155–171.

Davies, H.L., 1973. Fergusson Island 1:250,000. Geolog. Ser.–Explanatory Notes, Dep. Miner. Energy, Bur. Miner. Res. (Aust.).

————, 1980a. Crustal structure and emplacement of ophiolite in southeastern Papua New Guinea. Colloques Internationaux du C.N.R.S., 272:17–33.

————, 1980b. Folded thrust fault and associated metamorphics in the Suckling-Dayman Massif, Papua New Guinea. *Am. J. Sci.,* 280-A:171–191.

Davies, H.L., and Smith, I.E., 1971. Geology of eastern Papua. *Geol. Soc. Am. Bull.,* 82:3299–3312.

Davies, H.L., and Warren, R.G., 1988. Origin of eclogite-bearing, domed, layered metamorphic complexes ("core complexes") in the D'Entrecasteaux islands, Papua New Guinea. *Tectonics,* 7:1–21.

Fitzgerald, P.G., Muñoz, J.A., Coney, P.J., and Baldwin, S.L., 1999. Asymmetric exhu-mation across the Pyrenean orogen: implications for the tectonic evolution of col-lisional orogens. *Earth Planet. Sci. Lett.,* 173:157–170.

Galbraith, R.F., 1981. On statistical models for fission track counts. *Math. Geol.,* 13:471–478.

Goodliffe, A.M., Taylor, B., Martinez, F., Hey, R.N., Maeda, K., and Ohno, K., 1997. Synchronous reorientation of the Woodlark Basin spreading center. *Earth Planet. Sci. Lett.,* 146:233–242.

Green, P.F., 1981. A new look at statistics in fission-track dating. *Nucl. Tracks,* 5:77–86.

————, 1985. Comparison of zeta calibration baselines for fission-track dating of apatite, zircon and sphene. *Chem. Geol.,* 58:1–22.

Harrison, T.M., and McDougall, I., 1981. Excess ^{40}Ar in metamorphic rocks from Bro-ken Hill, New South Wales: implications for ^{40}Ar/^{39}Ar age spectra and the thermal history of the area. *Earth Planet. Sci. Lett.,* 55:123–149.

Hegner, E., and Smith, I.E.M., 1992. Isotopic compositions of late Cenozoic volcanics from southeast Papua New Guinea: evidence for multi-component sources in arc and rift environments. *Chem. Geol.,* 97:233–249.

Hill, E.J., 1994. Geometry and kinematics of shear zones formed during continental extension in eastern Papua New Guinea. *J. Struct. Geol.,* 16:1093–1105.

Hill, E.J., and Baldwin, S.L., 1993. Exhumation of high-pressure metamorphic rocks during crustal extension in the D'Entrecasteaux region: Papua New Guinea. *J. Metamorph. Geol.,* 11:261–277.

Hill, E.J., Baldwin, S.L., and Lister, G.S., 1992. Unroofing of active metamorphic core complexes in the D'Entrecasteaux Islands, Papua New Guinea. *Geology,* 20:907–910.

———, 1995. Magmatism as an essential driving force for formation of active metamorphic core complexes in eastern Papua New Guinea. *J. Geophys. Res.,* 100:10441–10451.

Hurford, A.J., and Green, P.F., 1983. The zeta age calibration of fission-track dating. *Chem. Geol.,* 41:285–317.

Lackschewitz, K., Mertz, D.F., Devey, C.W., Bogaard, P.V.D., and Garbe-Schoenberg, C.-D., 2001. Late Cenozoic volcanism in the western Woodlark Basin area, SW Pacific: implications by $^{40}Ar/^{39}Ar$, major and trace element, and Sr-Nd isotope data of marine volcanic ash layers [paper presented at ODP Conf., Karlsruhe, Germany, February 2001].

Laslett, G. M., Gleadow, A.J.W., and Duddy, I.R., 1984. The relationship between fission track length and density in apatite. *Nucl. Tracks,* 9:29–38.

Lus, W.Y., McDougall, I., and Davies, H.L., 1998. Emplacement age of the Papuan Ultramafic Belt Ophiolite: constraints from K-Ar and $^{40}Ar/^{39}Ar$ geochronology from hornblende granulites at the base of the ophiolite near the Musa-Kumusi divide. *In Geol.Soc. Austral. Abstracts No. 49.*

McDougall, I., and Harrison, T.M., 1999. *Geochronology and thermochronology by the $^{40}Ar/^{39}Ar$ method* (2nd ed.): Oxford (Oxford Univ. Press).

Monteleone, B., 2000. Thermochronologic constraints from the Moresby Seamount, Woodlark Basin, Papua New Guinea [M.S. thesis]. Univ. Ariz., Tucson.

Muir, R.J., Ireland, T.R., Weaver, S.D., and Bradshaw, J.D., 1996. Ion microprobe dating of Paleozoic granitoids: Devonian magmatism in New Zealand and correlations with Australia and Antarctica. *Chem. Geol. (Isot. Geosci.)* 127:191–210.

Paçes, J.B., and Miller, J.D., 1989. Precise U-Pb ages of Duluth Complex and related mafic intrusions, Northeastern Minnesota: Geochronological insights to physical, petrogenetic, paleomagnetic, and tectonomagmatic processes associated with the 1.1 Ga midcontinent rift system. *J. Geophys. Res.* 98:13997–14013.

Pringle, M.S., 1993. Age progressive volcanism in the Musicians Seamounts: a test of the hot-spot hypothesis for the Late Cretaceous Pacific. *In* Pringle, M.S., Sager, W.W., Sliter, W.V., and Stein, S. (Eds.), *The Mesozoic Pacific: Geology, Tectonics, and Volcanism.* Geophys. Monogr., Am. Geophys. Union, 77:187–215.

Robertson, A.H.F., Awadallah, S.A.M., Gerbaudo, S., Lackschewitz, K.S., Monteleone, B.D., Sharp, T.R., and Leg 180 Shipboard Party, in press. Sedimentary-tectonic evolution of the Miocene-Recent Woodlark basin, SW Pacific: implications for rift processes. *Spec. Publ.—Geol. Soc. London.* [N1]

Smith, I.E., and Simpson, C.J., 1972. Late Cenozoic uplift in the Milne Bay area, eastern Papua New Guinea. *Bull.—Bur. Miner. Resour., Geol. Geophys. (Aust.),* 125:29–35.

Smith, I.E.M., 1976. Peralkaline rhyolites from the D'Entrecasteaux Islands, Papua New Guinea. *In* Johnson, R.W. (Ed.), *Volcanism in Australasia:* Amsterdam (Elsevier), 275–285.

Smith, I.E.M., 1982. Volcanic evolution in eastern Papua. *Tectonophysics,* 87:315–333.

Steiger, R.H., and Jäger, E., 1977. Subcommission on geochronology: convention on the use of decay constants in geo- and cosmochronology. *Earth Planet. Sci. Lett.,* 36:359–362.

Stolz, A.J., Davies, G.R., Crawford, A.J., and Smith, I.E.M., 1993. Sr, Nd and Pb isotopic compositions of calc-alkaline and peralkaline silicic volcanics from the D'Entrecasteaux Islands, Papua New Guinea, and their tectonic significance. *Mineral. Petrol.,* 47:103–126.

Taylor, B., Goodliffe, A.M., and Martinez, F., 1999. How continents break up: insights from Papua New Guinea. *J. Geophys. Res.,* 104:7497–7512.

Taylor, B., Goodliffe, A., Martinez, F., and Hey, R., 1995. Continental rifting and initial sea-floor spreading in the Woodlark Basin. *Nature,* 374:534–537.

Taylor, B., Huchon, P., Klaus, A., et al., 1999. *Proc. ODP, Init. Repts.,* 180 [CD-ROM]. Available from: Ocean Drilling Program, Texas A&M University, College Station, TX 77845-9547, U.S.A.

Tregoning, P., Lambeck, K., Stolz, A., Morgan, P., McClusky, S., van der Beek, P., McQueen, H., Jackson, R., Little, R., Laing, A., and Murphy, B., 1998. Estimation of current plate motions in Papua New Guinea from global positioning system observations. *J. Geophys. Res.,* 103:12,181–12,203.

Walker, D.A., and McDougall, I., 1982. $^{40}Ar/^{39}Ar$ and K-Ar dating of altered glassy volcanic rocks: the Dabi Volcanics. *Geochim. Cosmochim. Acta,* 46:2181–2190.

Weissel, J.K., Taylor, B., and Karner, G.D., 1982. The opening of the Woodlark basin, subduction of the Woodlark spreading system, and the evolution of northern Melanesia since mid-Pliocene time. *Tectonophysics,* 87:253–277.

Figure F1. Map of eastern Papua New Guinea and the Solomon Islands showing present-day tectonic setting (after Taylor et al., 1995). MS = Moresby Seamount, PNG = Papua New Guinea. The cross section (A–B) in the Moresby Seamount area is shown in Figure F2, p. 19.
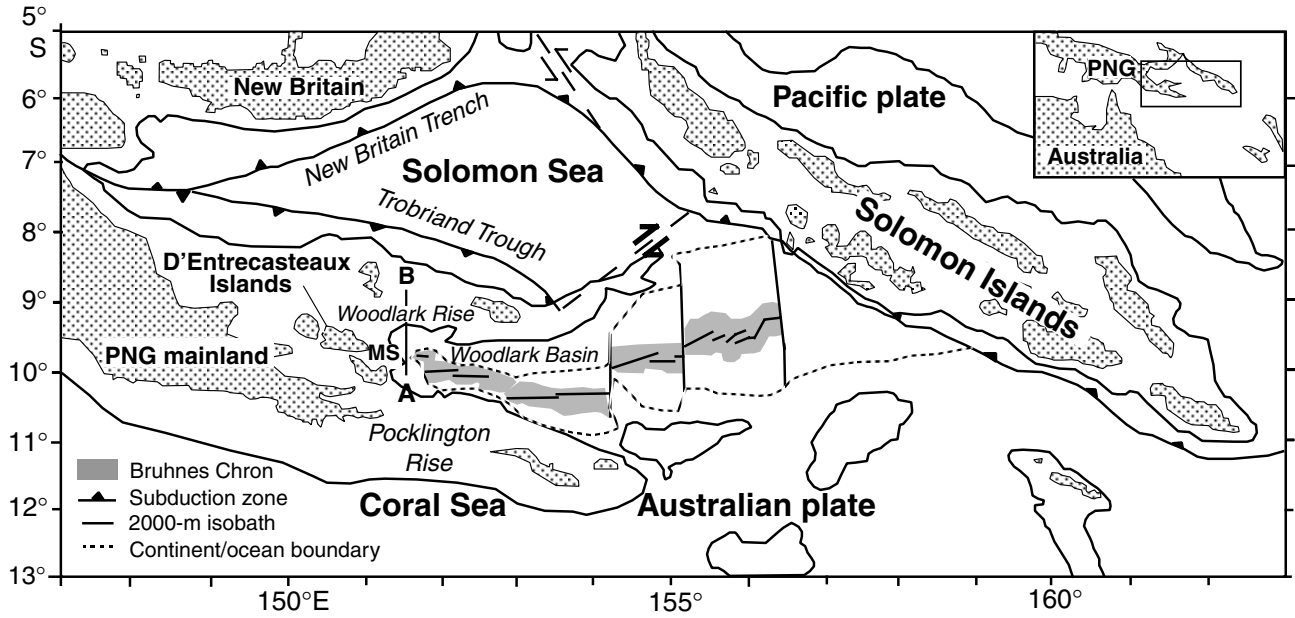
Figure F2. Cross section at 151°34.5′E showing the bathymetry and structures in the vicinity of the Moresby Seamount, Leg 180 drill sites, and lithostratigraphy of Sites 1108–1118 (after Taylor, Huchon, Klaus, et al., 1999). MS = Moresby Seamount, VE = vertical exaggeration.
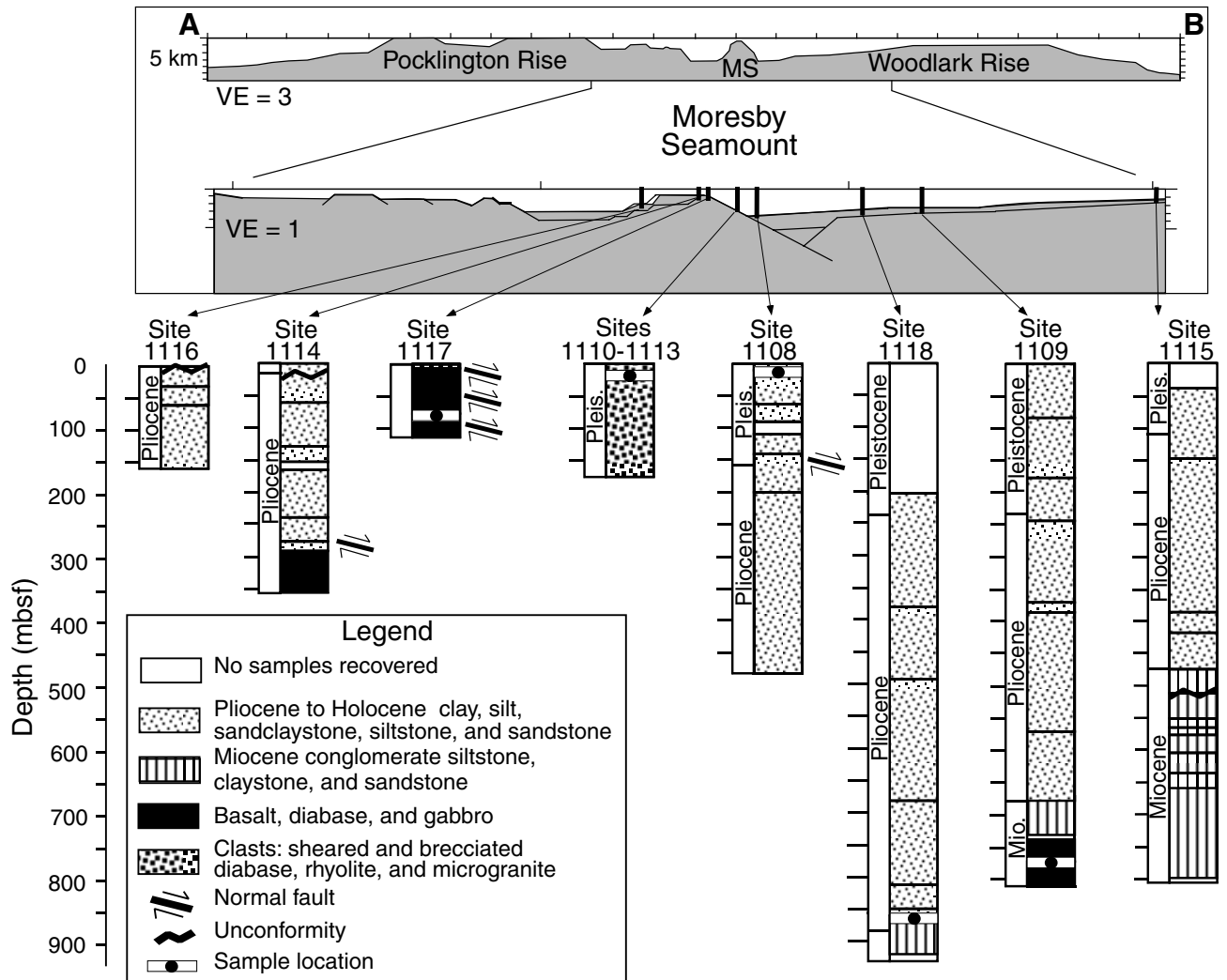
Figure F3. A. $^{40}Ar/^{39}Ar$ age spectrum and $(^{39}Ar)_K/(^{37}Ar)_{Ca}$ plot for Core 180-1109D-45R. White apparent age spectrum assumes an atmospheric $(^{40}Ar/^{36}Ar)_i = 295.5$, the black spectrum is corrected using $(^{40}Ar/^{36}Ar)_i = 323.8 \pm 7.7$ from the isochron plot. **B.** Isochron plot for plagioclase Core 180-1109D-45R. MSWD = mean squared weighted deviates.
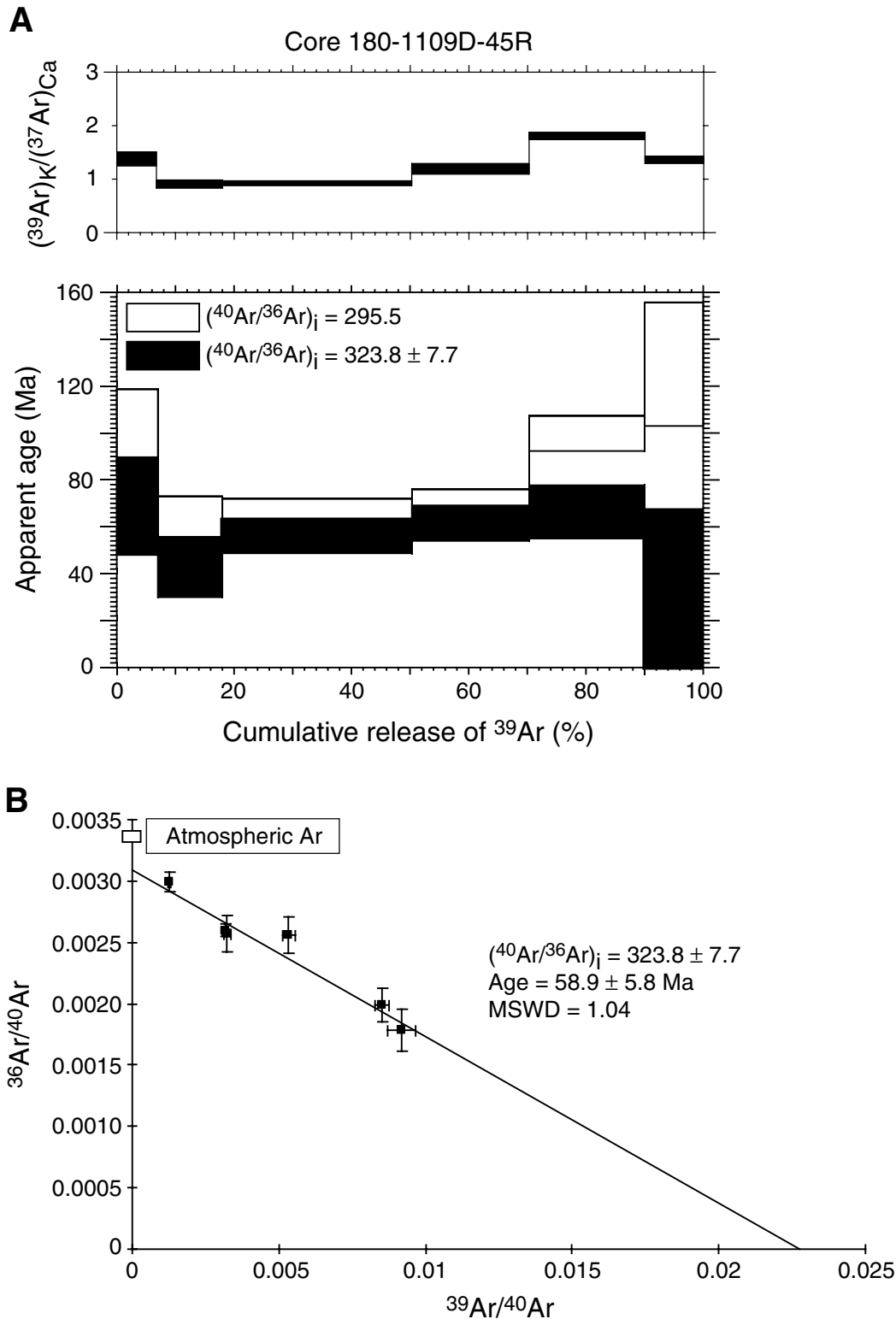
Figure F4. A. $^{40}Ar/^{39}Ar$ age spectrum and $(^{39}Ar)_K/(^{37}Ar)_{Ca}$ plot for Core 180-1118A-70R step heat experiment. **B.** Isochron plot for Sample 180-1118A-70R plagioclase step heat experiment. MSWD = mean squared weighted deviates.

A

Core 180-1118A-70R

$(^{40}Ar/^{36}Ar)_i = 295.5$

B

Atmospheric Ar

$(^{40}Ar/^{36}Ar)_i = 300.8 \pm 1.8$
Age = 31.0 $\pm$ 0.9 Ma
MSWD = 2.58
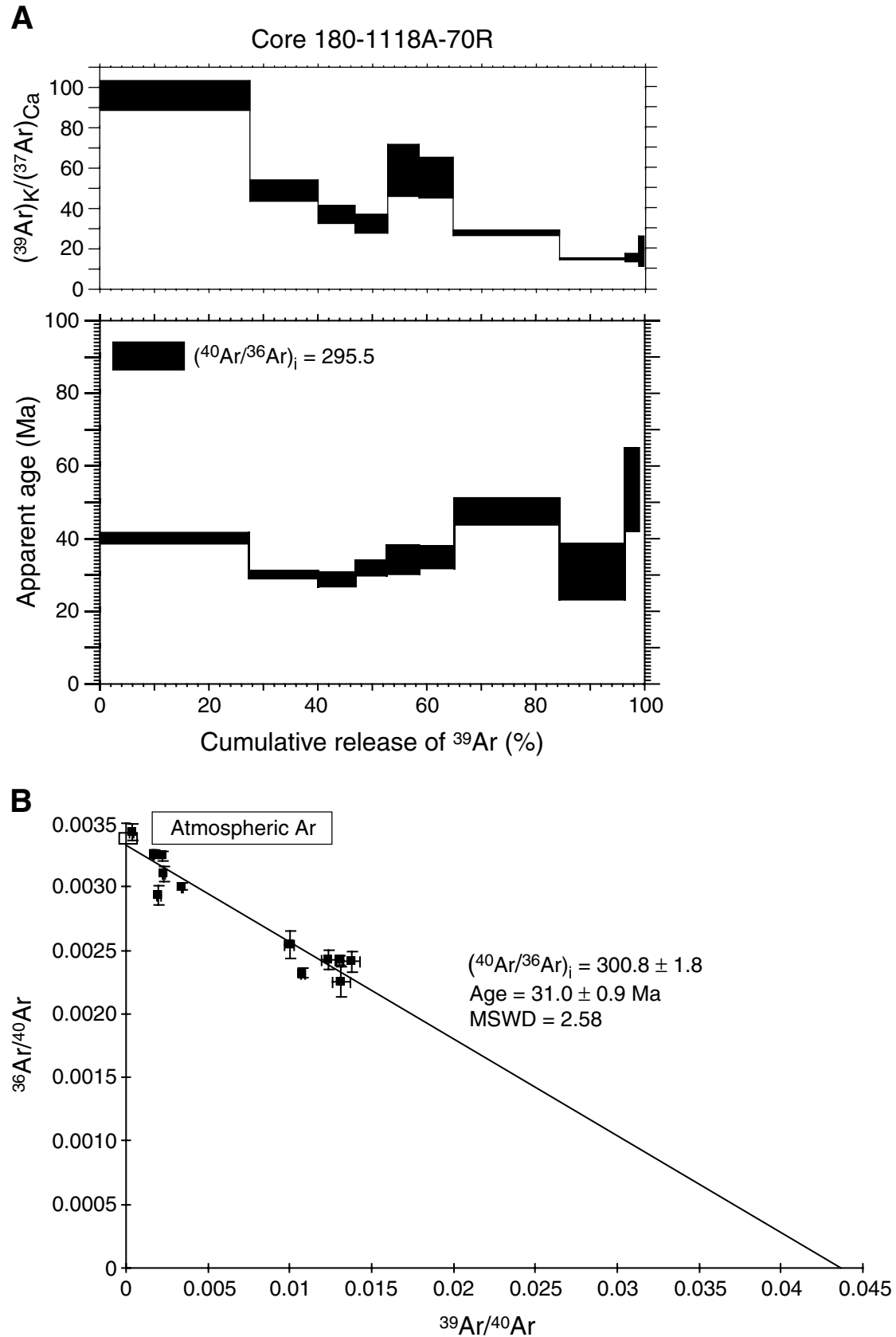
Figure F5. A. $^{40}Ar/^{39}Ar$ age spectrum and $(^{39}Ar)_K/(^{37}Ar)_{Ca}$ plot for Core 180-1117A-11R. White age spectrum assumes atmospheric $(^{40}Ar/^{36}Ar)_i = 295.5$, the black spectrum is corrected using $(^{40}Ar/^{36}Ar)_i = 355.4 \pm 4.2$ from the isochron plot. **B.** Isochron plot for Core 180-1117A-11R plagioclase step heat experiment. MSWD = mean squared weighted deviates.
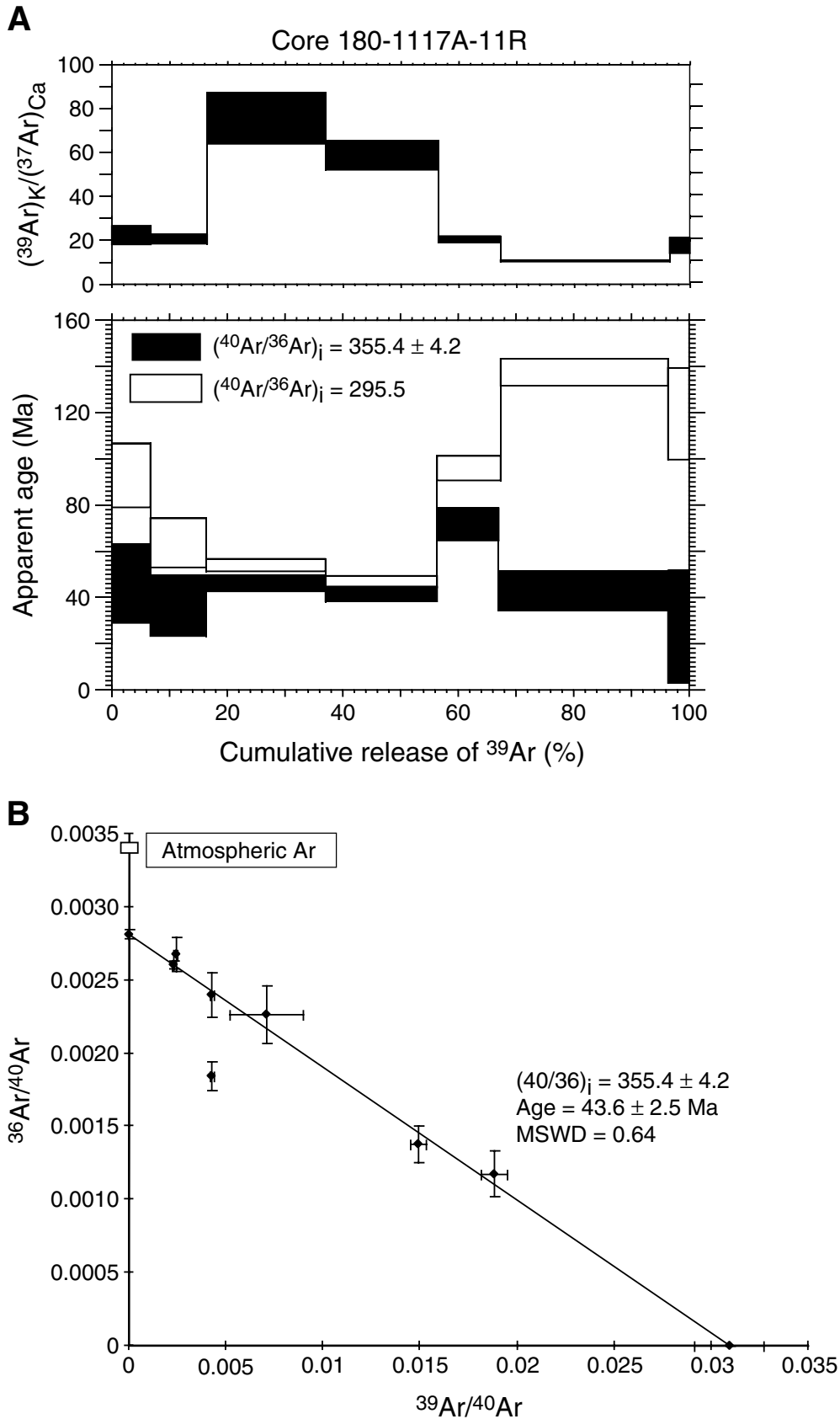
Figure F6. A. ^{40}Ar/^{39}Ar age spectrum and $(^{39}$Ar$)_K/(^{37}$Ar$)_{Ca}$ plot for Core 180-1117-alt. The separate contained highly altered plagioclase grains. The white spectrum is corrected assuming an atmospheric $(^{40}$Ar/^{36}Ar$)_i =$ 295.5, the black spectrum is corrected using $(^{40}$Ar/^{36}Ar$)_i = 392.3 \pm 8.7$ from the isochron plot. **B.** Isochron plot for Core 180-1117-alt plagioclase step heat experiment. MSWD = mean squared weighted deviates.
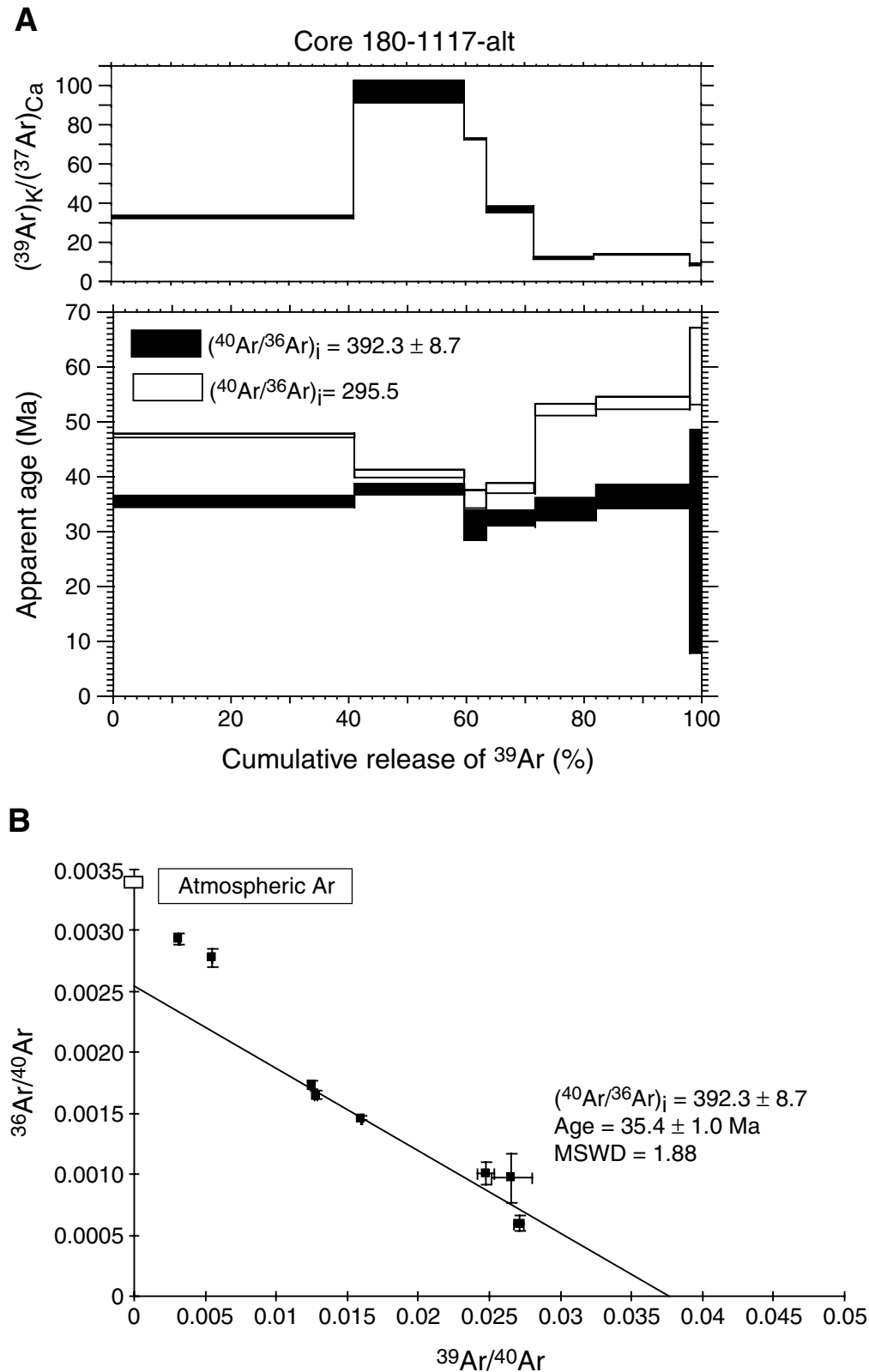
Figure F7. Tera-Wasserburg plot for Sample 180-1117A-11R gabbro. See **"U/Pb Results,"** p. 9, in "Basalt, Diabase, and Gabbro" in "Results and Interpretation" for discussion.
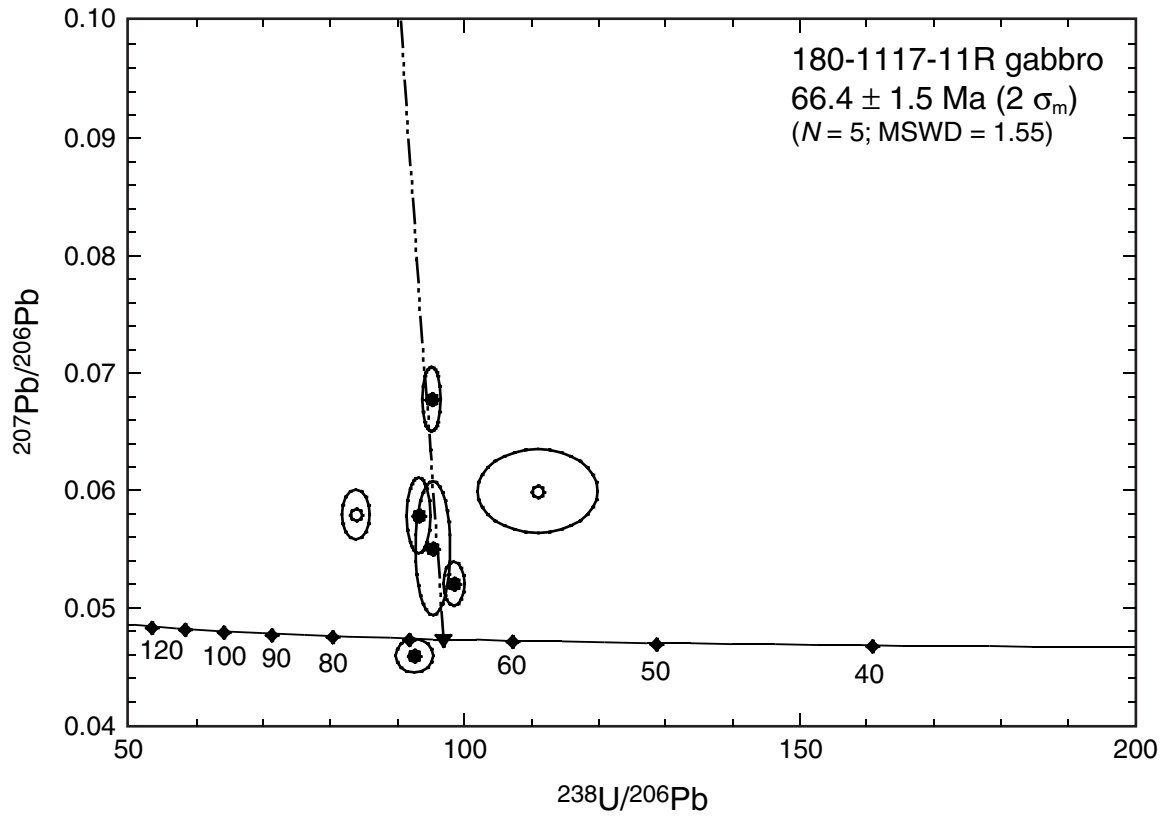
Figure F8. ^{40}Ar/^{39}Ar age spectrum for single grain of K-feldspar (Core 180-1110B-3X).
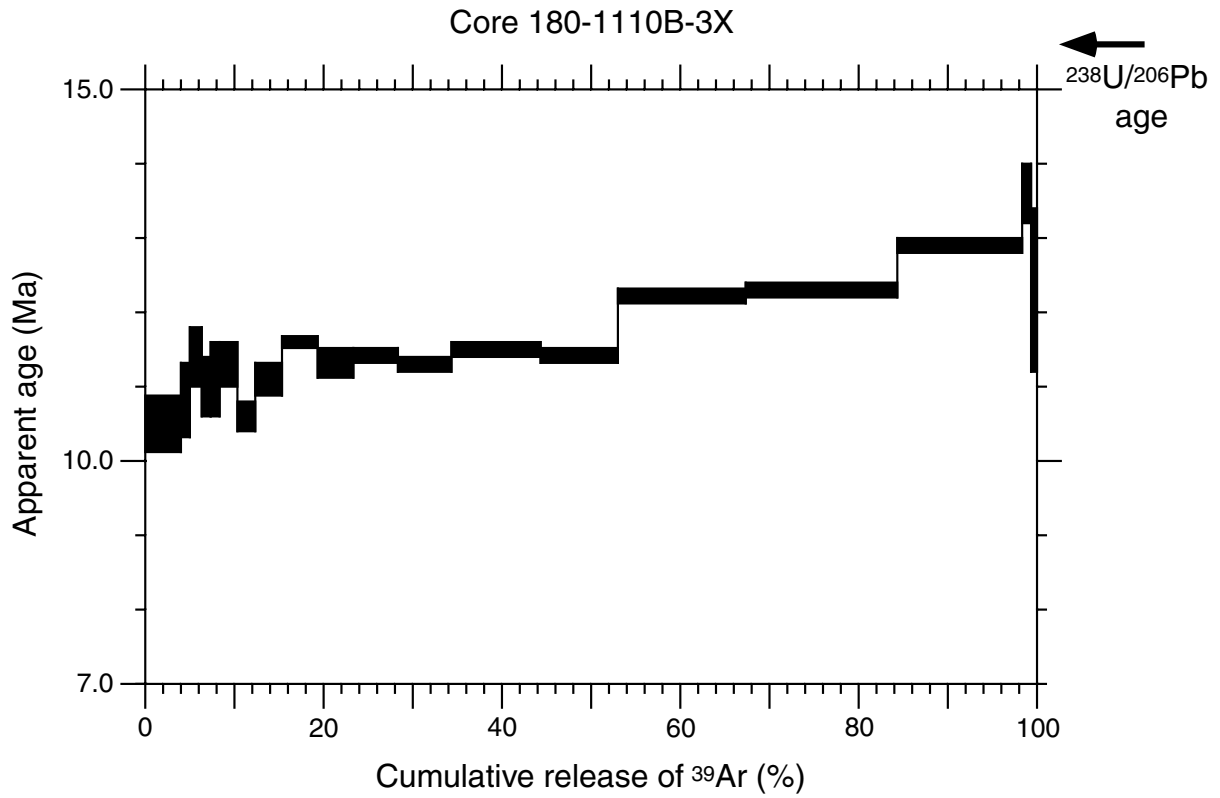
Core 180-1110B-3X

Figure F9. $^{40}Ar/^{39}Ar$ age spectrum for single grain of K-feldspar (Core 180-1111A-16R).
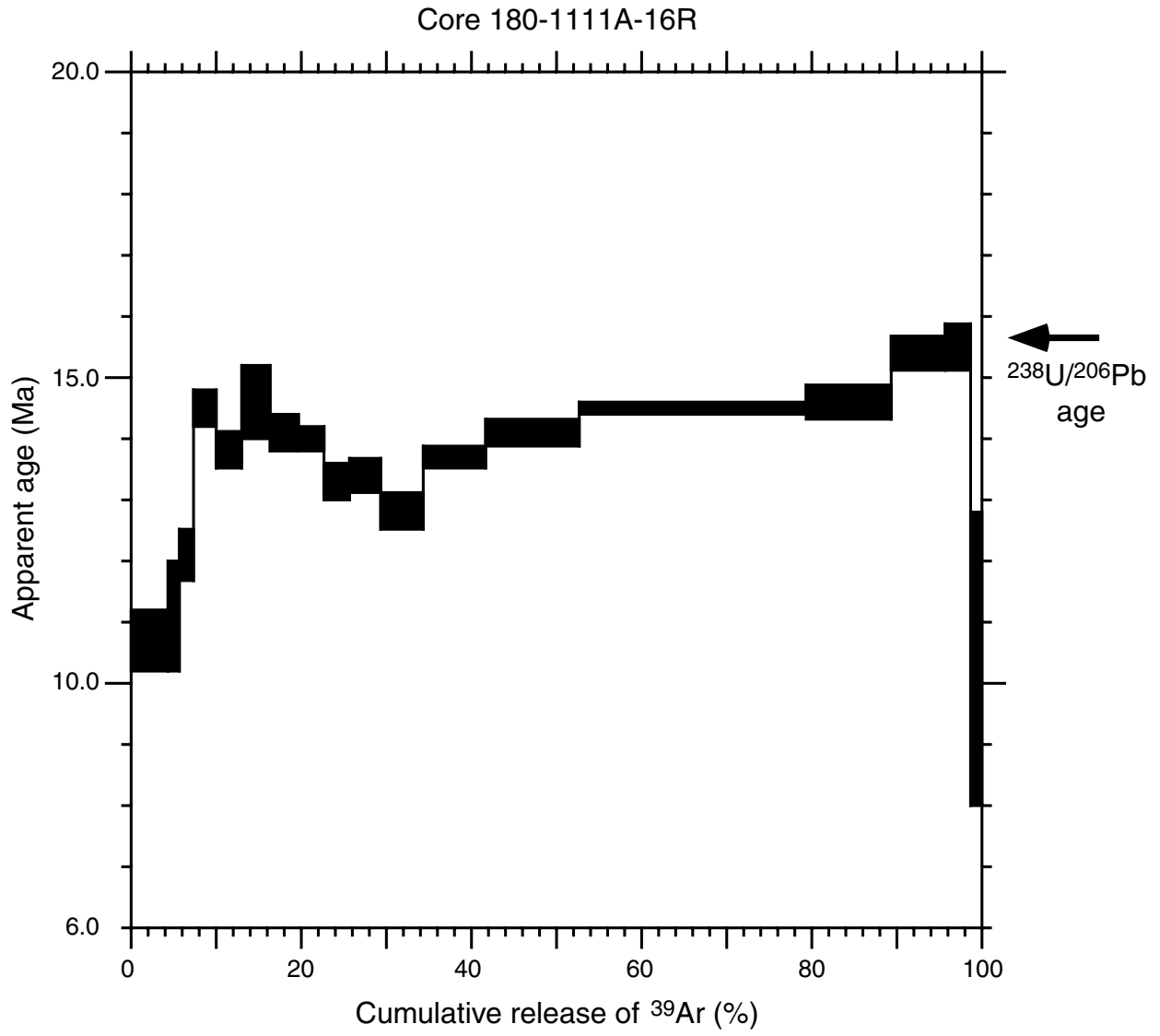
Core 180-1111A-16R

Figure F10. Tera-Wasserburg plot of zircons from Cores 180-1108B-6R (square), 180-1110B-3X (circles), and 180-1111A-16R (triangles). Zircons from rhyolite clasts gave an age of 15.7 ± 0.4 Ma (MSWD = mean squared weighted deviates), and zircons from a microgranite clast gave $^{238}U/^{206}Pb$ ages of 3.1 and 550 Ma.
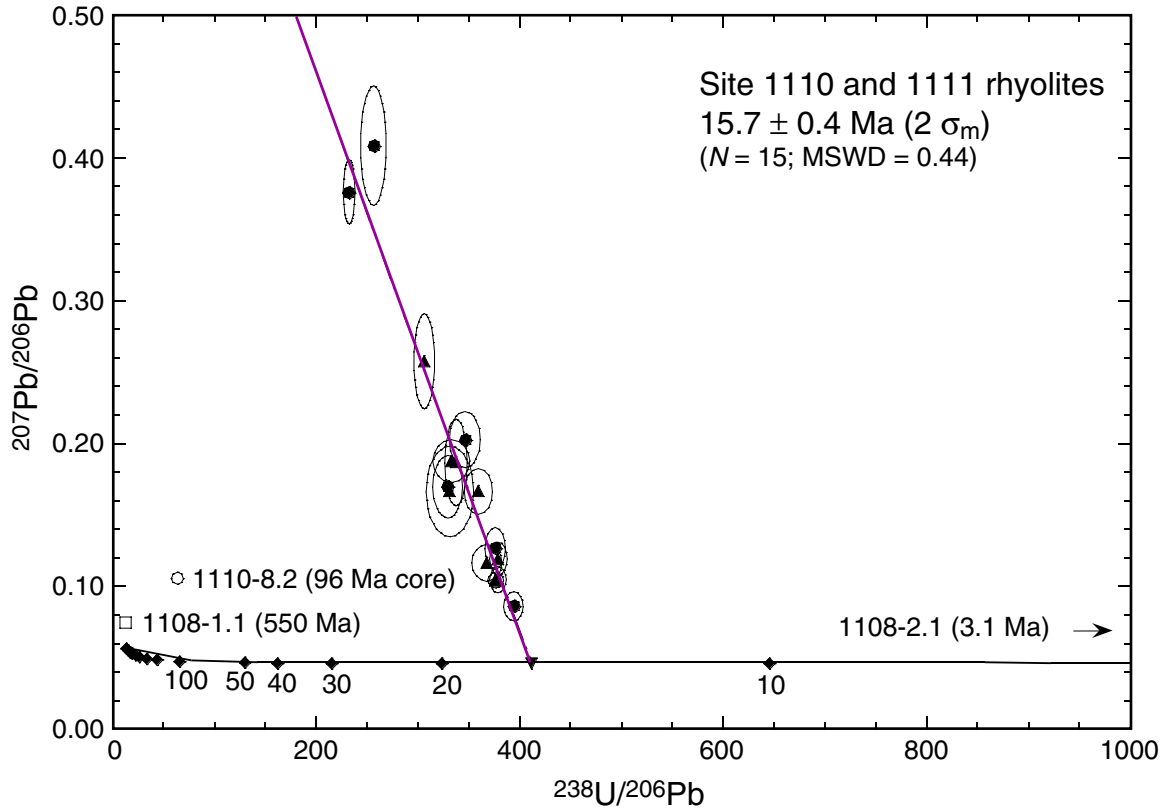
Figure F11. Plot of $^{40}Ar/^{39}Ar$ isochron age vs. increasing degree of alteration for plagioclase samples analyzed in this study.
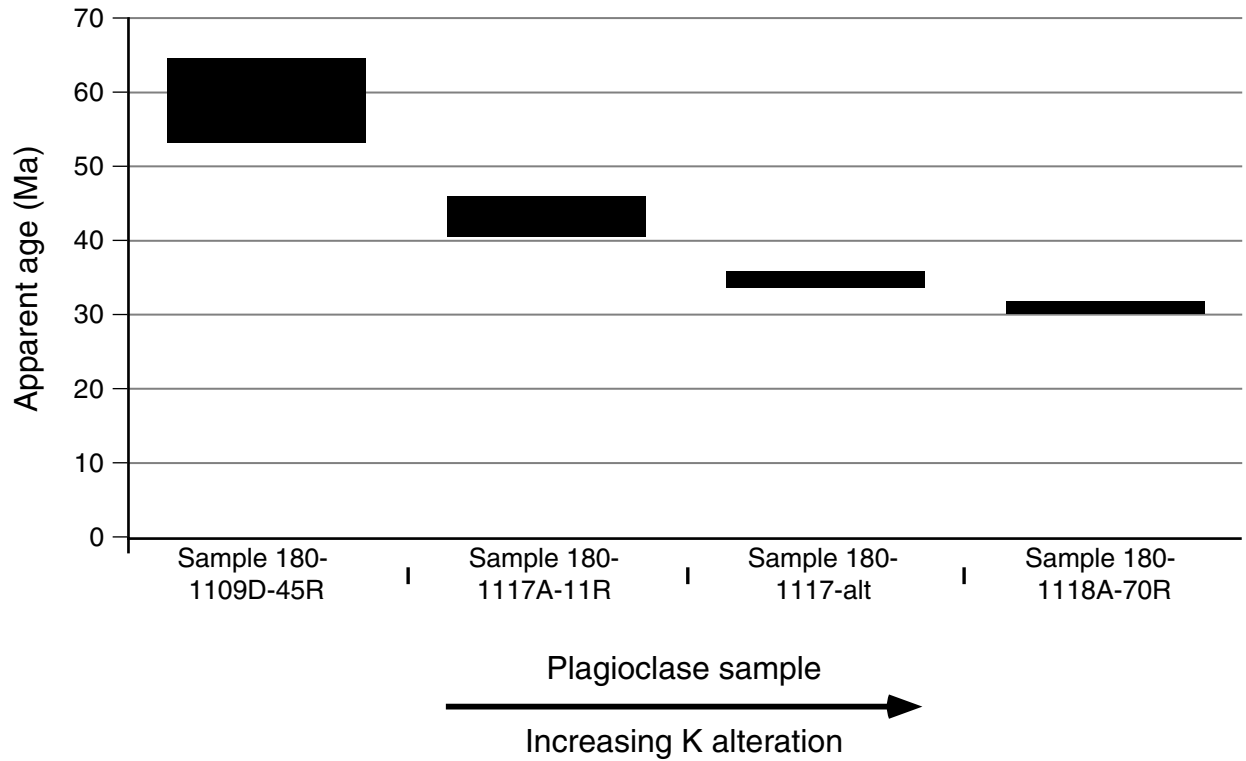
Table T1. Summary of thermochronological results, Leg 180.

Hole, core	Rock type	Mineral	Analysis	Age (Ma)	Comments
180-1109D-					
45R	Diabase	Plagioclase	$^{40}Ar/^{39}Ar$–TF	161.1 ± 35.1	No K alteration
45R	Diabase	Plagioclase	$^{40}Ar/^{39}Ar$–SH	58.9 ± 5.8	Unaltered, plagioclase cooling age
180-1117A-					
11R	Gabbro	Zircon	$^{238}U/^{206}Pb$	66.4 ± 1.5	Thin section, crystallization age
11R	Gabbro	Plagioclase	$^{40}Ar/^{39}Ar$–TF	51.4 ± 22.6	Moderate K alteration
11R	Gabbro	Plagioclase	$^{40}Ar/^{39}Ar$–SH	43.6 ± 2.5	Moderate K alteration
alt	Gabbro	Plagioclase	$^{40}Ar/^{39}Ar$–TF	54.7 ± 3.7	More altered 1117 separate
alt	Gabbro	Plagioclase	$^{40}Ar/^{39}Ar$–SH	35.4 ± 1.0	More altered 1117 separate
180-1118A-					
70R	Diabase	Plagioclase	$^{40}Ar/^{39}Ar$–TF	32.7 ± 5.8	Pervasive K alteration, K alteration age
70R	Diabase	Plagioclase	$^{40}Ar/^{39}Ar$–SH	31.0 ± 0.9	Pervasive K alteration, K alteration age
180-1110B-					
3X	Rhyolite	K-feldspar	$^{40}Ar/^{39}Ar$–TF	12.5 ± 0.2	K-feldspar altered to sericite
3X	Rhyolite	K-feldspar	$^{40}Ar/^{39}Ar$–SH	11.9 ± 0.2	K-feldspar altered to sericite, hydrothermal alteration 10–11 Ma
3X	Rhyolite	Zircon	$^{238}U/^{206}Pb$	15.7 ± 0.3	Mineral separate, crystallization age of arc-related volcanics
180-1111A-					
16R	Rhyolite	K-feldspar	$^{40}Ar/^{39}Ar$–TF	14.4 ± 0.6	K-feldspar altered to sericite
16R	Rhyolite	K-feldspar	$^{40}Ar/^{39}Ar$–SH	14.1 ± 0.3	K-feldspar altered to sericite, hydrothermal alteration 10–11 Ma
16R	Rhyolite	Zircon	$^{238}U/^{206}Pb$	15.7 ± 0.3	Mineral separate, crystallization age of arc-related volcanics
180-1108B-					
6R	Microgranite	Biotite	$^{40}Ar/^{39}Ar$–TF	2.6 ± 0.2	Some chlorite contamination, biotite cooling age
6R	Microgranite	Feldspar	$^{40}Ar/^{39}Ar$–TF	2.1 ± 0.3	Unaltered, mixture of albite and microcline, feldspar cooling age
6R	Microgranite	Zircon	$^{238}U/^{206}Pb$	3.1 ± 0.1	Two generations of zircon, 3 Ma zircon represents crystallization age
				550 ± 12	
6R	Microgranite	Apatite	Fission Track	2.7 ± 1.2	Apatite rapid cooling age

Note: TF = total fusion, SH = step heat.

Table T2. ^{40}Ar/^{39}Ar analytical results. (See table notes. Continued on next two pages.)

Hole, core	Mineral	J	Weight (g)	Grain size (µm)	Temp (°C)	^{40}Ar/^{39}Ar[†]	^{37}Ar/^{39}Ar[‡]	^{36}Ar/^{39}Ar[†]	^{39}Ar$_k$ (counts)**	Cumulative ^{39}Ar released (%)	^{40}Ar*[‡] (%)	^{40}Ar*/^{39}Ar$_K$	Age (Ma)	± 1 σ
180-1110B-3X	K-feldspar	0.00076393	0.012126	single grain										
					450	73.870	0.201	0.227	6958	2.91	9.9	7.31	10.0	0.9
					470	15.392	0.738	0.027	2816	4.08	49.8	7.66	10.5	0.4
					490	13.074	1.096	0.018	2510	5.13	60.4	7.88	10.8	0.5
					520	12.638	1.253	0.015	3000	6.39	65.9	8.32	11.4	0.4
					550	12.464	0.599	0.015	1924	7.19	64.4	8.02	11.0	0.4
					600	16.423	0.245	0.028	2991	8.44	49.3	8.1	11.1	0.5
					650	13.672	0.089	0.018	4549	10.34	60.5	8.26	11.3	0.3
					700	11.007	0.031	0.011	4612	12.27	70	7.69	10.6	0.2
					775	11.083	0.015	0.010	7256	15.3	72.9	8.06	11.1	0.2
					850	10.246	0.056	0.006	9955	19.46	82.6	8.44	11.6	0.1
					890	10.777	0.003	0.009	9469	23.42	76.3	8.21	11.3	0.2
					930	11.322	0.004	0.010	11755	28.33	73.2	8.27	11.4	0.1
					970	11.703	0.003	0.012	14572	34.42	70.6	8.24	11.3	0.1
					1010	11.885	0.002	0.012	24044	44.47	70.4	8.34	11.5	0.1
					1035	11.859	0.001	0.012	20479	53.03	70.4	8.33	11.4	0.1
					1060	11.945	0.001	0.011	34425	67.42	74.3	8.85	12.2	0.1
					1080	12.000	0.001	0.010	40600	84.39	74.7	8.95	12.3	0.1
					1130	12.109	0.001	0.009	33518	98.39	77.9	9.41	12.9	0.1
					1180	14.713	0.000	0.016	2468	99.43	67.5	9.91	13.6	0.4
					1300	20.976	0.005	0.041	1246	99.95	42.7	8.95	12.3	1.1
					1500	2828.098	0.138	9.389	100	99.99	2.8	79.42	106.3	46.7
					1600	11427.723	0.128	38.861	27	100.00	0.4	50.83	68.7	122.2
												Integrated Age = 11.9 ± 0.2 Ma		
1111A-16R	K-feldspar	0.00076335	0.011378	single grain										
					450	113.668	0.051	0.354	5293	2.87	8.7	9.93	13.6	1.4
					480	22.440	0.131	0.050	2607	4.29	34.9	7.81	10.7	0.5
					510	19.224	0.127	0.038	2270	5.52	42.0	8.05	11.1	0.9
					550	18.721	0.078	0.034	3377	7.35	47.3	8.85	12.1	0.4
					600	22.836	0.011	0.042	4751	9.93	46.4	10.58	14.5	0.3
					650	18.244	0.008	0.028	5395	12.86	55.2	10.05	13.8	0.3
					700	41.701	0.006	0.106	6405	16.33	25.6	10.66	14.6	0.6
					750	15.956	0.008	0.019	6035	19.61	64.5	10.27	14.1	0.3
					800	15.814	0.005	0.019	5675	22.69	64.8	10.23	14.0	0.2
					850	19.712	0.005	0.034	5777	25.82	49.2	9.68	13.3	0.3
					900	24.505	0.009	0.050	6509	29.36	39.8	9.74	13.4	0.3
					950	22.650	0.007	0.046	8974	34.23	41.2	9.32	12.8	0.3
					990	21.944	0.006	0.041	13437	41.52	45.7	10.01	13.7	0.2
					1020	22.397	0.004	0.041	20514	52.65	45.8	10.25	14.1	0.2
					1050	19.220	0.005	0.029	49135	79.31	55.2	10.58	14.5	0.1
					1080	19.523	0.003	0.030	18617	89.42	54.3	10.63	14.6	0.3
					1150	20.439	0.004	0.031	11546	95.68	55.0	11.23	15.4	0.3
					1300	18.141	0.004	0.023	5644	98.75	62.5	11.32	15.5	0.4
					1500	166.899	0.005	0.544	2312	100.00	4.5	7.57	10.4	2.4
												Integrated Age = 14.1 ± 0.3 Ma		

Table T2 (continued).

Hole, core	Mineral	J	Weight (g)	Grain size (µm)	Temp (°C)	$^{40}Ar/^{39}Ar^\dagger$	$^{37}Ar/^{39}Ar^\ddagger$	$^{36}Ar/^{39}Ar^\dagger$	$^{39}Ar_k$ (counts)**	Cumulative ^{39}Ar released (%)	$^{40}Ar*^\ddagger$ (%)	$^{40}Ar*/^{39}Ar_K$	Age (Ma)	± 1 σ
1109D-45R	Plagioclase	0.00075457	0.014988	106–150										
					450	802.398	39.214	102.144	13	1.25	–0.3	–102.4	—	103.4
					600	288.718	67.316	0.760	56	6.8	24.6	76.3	98.4	18.2
					700	168.474	98.485	0.456	113	18.0	24.9	46.7	60.5	10.7
					850	105.678	97.350	0.234	327	50.2	41.7	49.1	64.3	6.2
					950	100.245	77.242	0.198	201	70.2	47.7	52	69.3	6.6
					1100	300.400	52.278	0.795	201	90.0	23.7	75.4	98.9	7.6
					1300*	748.150	68.171	2.259	139	100.0	12.2	98.6	128.8	26.6
												Integrated Age = 79.3 ± 11.0 Ma		
1117A-11R	Plagioclase	0.00075585	0.014965	106–150										
					450	3758.641	0.479	12.280	58	2.48	4.4	163.4	210.1	56.6
					600	232.905	4.461	0.559	101	6.82	29.9	69.8	92.8	13.9
					700	140.379	4.839	0.319	226	16.46	33.7	47. 5	63.7	10.6
					850	67.217	1.320	0.093	483	37.1	59.7	40.1	53.9	2.7
					950	53.154	1.701	0.063	452	56.41	65.6	34.8	46.9	2.5
					1050	156.368	4.862	0.289	253	67.22	46.1	72.3	96.0	5.4
					1300	436.823	9.244	1.140	683	96.41	23.8	104.8	137.5	5.7
					1500	415.226	5.630	1.112	84	100	21.7	90.6	119.5	19.7
												Integrated Age = 90.4 ± 7.0 Ma		
1117-alt	Plagioclase	0.000774677	0.013526	106–150										
					450	182.914	6.582	0.510	593	4.44	18.6	34.2	45.5	5.3
					600	62.599	3.030	0.093	4882	41.0	57.1	35.8	47.5	0.8
					700	37.008	1.031	0.023	2490	59.7	82.4	30.5	40.6	0.9
					850	37.735	1.382	0.037	506	63.4	71.5	27.0	35.9	1.7
					950	40.416	2.706	0.042	1093	71.6	71.1	28.4	37.9	1.0
					1100	79.461	8.203	0.140	1364	81.8	49.2	39.3	52.2	1.3
					1300	77.859	7.197	0.131	2153	98.0	51.4	40.2	53.4	1.3
					1500	318.558	11.183	0.938	272	100.0	14.1	45.3	60.1	7.0
												Integrated Age = 46.6 ± 1.3 Ma		
1118A-70R	Plagioclase	0.0007567	0.013546	75–106										
					450	598.933	0.511	1.959	334	3.74	4.5	27.2	34.6	9.5
					600	93.127	1.040	0.217	2094	27.2	31.9	29.7	39.9	1.5
					700	76.929	2.042	0.188	1148	40.12	28.9	22.3	29.6	1
					775	72.863	2.686	0.179	602	46.87	29.2	21.3	27.9	1.8
					850	80.975	3.061	0.199	525	52.8	28.9	23.5	31.0	2
					925	100.479	1.696	0.260	522	58.6	25.2	25.3	33.2	3.9
					1000	76.316	1.805	0.174	555	64.9	33.9	25.8	34.5	3.1
					1100	294.640	3.560	0.890	1736	84.3	11.9	35.2	47.3	3.7
					1175	458.102	6.595	1.490	1061	96.2	5.0	22.8	30.6	7.6
					1250	439.110	6.309	1.372	235	98.9	9.0	39.8	51.5	11.5
					1375	510.220	5.260	1.513	73	99.7	13.9	71.2	90.8	22.1
					1500	3278.937	14.120	11.309	28	100	–0.5	–16.9	—	23.1
												Integrated Age = 37.2 ± 3.7 Ma		

Table T2 (continued).

Hole, core	Mineral	J	Weight (g)	Grain size (µm)	Temp (°C)	$^{40}Ar/^{39}Ar$[†]	$^{37}Ar/^{39}Ar$[‡]	$^{36}Ar/^{39}Ar$[†]	$^{39}Ar_K$ (counts)**	Cumulative ^{39}Ar released (%)	$^{40}Ar^*$[‡] (%)	$^{40}Ar^*/^{39}Ar_K$	Age (Ma)	± 1 σ
Total Fusion Analyses														
1108B-6R	Feldspar	0.00089726	0.00162	75–106	1500	11.10	0.12	0.03	10020	100	11.7	1.3	2.1	0.3
1108B-6R	Biotite	0.00090429	0.001398	75–106	1350	9.62	0.04	0.03	6800	100	16.3	1.56	2.6	0.2
1109D-45R	Plagioclase	0.00075439	0.001064	106–150	1500	1103.916	67.971	3.392	110	100	10.5	123.8	161.1	35.1
1117A-11R	Plagioclase	0.00075532	0.000835	106–150	1500	1472.471	5.305	4.901	150	100	2.6	38.3	51.4	22.6
1117-alt	Plagioclase	0.00075180	0.001078	106–150	1500	176.672	3.804	0.465	920	100	23.1	40.9	54.7	3.7
1118A-70R	Plagioclase	0.00075655	0.001134	75–106	1500	4194.136	3.003	1.351	641	100	5.74	24.1	32.7	5.8
1110B-03X	K-feldspar	0.00076129	0.001248	whole grain	1500	20.378	0.043	0.038	24275	100	44.9	9.14	12.5	0.2
1111A-16R	K-feldspar	0.00076513	0.000883	whole grain	1500	56.320	0.004	0.157	16122	100	18.6	10.5	14.4	0.6

Notes: J = irradiation parameter. λ = 5.543 × 10^{-10}/yr. * = 1500°C step yielded insufficient amount of argon for age calculation, † = corrected for line blank, ‡ = corrected for line blank and ^{37}Ar decay, ** = sensitivity based on air aliquot 3.965 × 10^{-14} mol/count. Correction factors used to account for interfering nuclear reactions for all samples except Core 180-1108B-6R feldspar and biotite (see below) are: $(^{36}Ar/^{37}Ar)_{Ca}$ = 0.000242 ± 0.000084, $(^{38}Ar/^{37}Ar)_{Ca}$ = 0.00193 ± 0.000042, $(^{39}Ar/^{37}Ar)_{Ca}$ = 0.0010709 ± 0.0001023, $(^{40}Ar/^{39}Ar)_K$ = 0.0199 ± 0.0087, $(^{38}Ar/^{39}Ar)_K$ = 0.012542 ± 0.000057. Correction factors used to account for interfering nuclear reactions for Core 180-1108B-6R feldspar and biotite are: $(^{36}Ar/^{37}Ar)_{Ca}$ = 0.00045 ± 0.00015, $(^{38}Ar/^{37}Ar)_{Ca}$ = 0.00042 ± 0.00014, $(^{39}Ar/^{37}Ar)_{Ca}$ = 0.00118 ± 0.0004, $(^{40}Ar/^{39}Ar)_K$ = 0.0416 ± 0.0054, $(^{38}Ar/^{39}Ar)_K$ = 0.0163 ± 0.0001.

Table T3. U/Pb analytical results.

Label	U (ppm)	Th (ppm)	Th/U	$^{204}Pb/^{206}Pb$	$^{207}Pb/^{206}Pb$	$^{238}U/^{206}Pb$	Age* (Ma)
Site 1110 rhyolite							
1.1	214	3	0.02	0.0332 ± 0.0046	0.377 ± 0.023	230.7 ± 6.0	16.2 ± 0.9
2.1	335	22	0.07	0.0039 ± 0.0066	0.087 ± 0.010	392.5 ± 9.8	15.6 ± 0.4
4.1	74	1	0.02	0.0218 ± 0.0202	0.410 ± 0.042	254.8 ± 12.6	13.6 ± 1.5
5.1	180	9	0.05	0.0107 ± 0.0122	0.204 ± 0.020	345.0 ± 15.0	14.9 ± 0.8
7.1	155	48	0.31	0.0087 ± 0.0192	0.171 ± 0.022	327.7 ± 14.3	16.5 ± 0.9
8.1	398	18	0.05	0.0000 ± 0.0038	0.128 ± 0.015	374.6 ± 10.1	15.4 ± 0.5
8.2	75	26	0.35	0.0031 ± 0.0041	0.107 ± 0.005	62.0 ± 1.8	95.5 ± 2.8[†]
Site 1111 rhyolite							
1.1	464	29	0.06	0.0077 ± 0.0051	0.105 ± 0.009	376.9 ± 8.3	15.8 ± 0.4
2.1	406	26	0.07	0.0021 ± 0.0036	0.120 ± 0.011	377.7 ± 9.0	15.4 ± 0.4
3.1	123	7	0.06	0.0062 ± 0.0111	0.168 ± 0.032	329.8 ± 23.1	16.5 ± 1.4
4.1	465	130	0.28	0.0045 ± 0.0047	0.105 ± 0.005	374.7 ± 7.8	15.9 ± 0.3
5.1	376	24	0.06	0.0027 ± 0.0051	0.117 ± 0.013	366.1 ± 14.5	16.0 ± 0.7
6.1	181	11	0.07	0.0050 ± 0.0078	0.189 ± 0.015	331.2 ± 18.4	15.9 ± 1.0
7.1	223	18	0.08	0.0039 ± 0.0070	0.188 ± 0.030	336.0 ± 10.7	15.7 ± 0.9
8.1	151	2	0.01	0.0051 ± 0.0097	0.259 ± 0.033	304.7 ± 10.3	15.4 ± 1.0
9.1	235	5	0.02	0.0071 ± 0.0068	0.167 ± 0.016	357.9 ± 13.8	15.2 ± 0.7
Site 1108 microgranite							
1.1	116	78	0.67	0.0013 ± 0.0009	0.075 ± 0.002	11.0 ± 0.2	550 ± 12
2.1	1448	664	0.46	0.0071 ± 0.0069	0.072 ± 0.013	1999.4 ± 54.3	3.1 ± 0.1
Site 1117A-11R gabbro							
3.1	2028	8328	4.11	0.0011 ± 0.0005	0.068 ± 0.003	94.9 ± 1.4	65.8 ± 1.0
5.1	7609	29605	3.89	0.0011 ± 0.0004	0.058 ± 0.002	83.6 ± 2.0	75.6 ± 1.8[†]
6.1	2716	18890	6.95	0.0006 ± 0.0006	0.060 ± 0.004	110.7 ± 8.9	57.0 ± 4.6[†]
8.1	656	2099	3.20	0.0029 ± 0.0011	0.055 ± 0.006	95.1 ± 2.5	66.8 ± 1.8
10.1	1509	2912	1.93	0.0004 ± 0.0004	0.052 ± 0.002	98.2 ± 1.6	64.9 ± 1.1
13.1	1981	7874	3.97	0.0010 ± 0.0006	0.058 ± 0.003	92.9 ± 1.8	68.1 ± 1.3
15.1	3159	9440	2.99	0.0001 ± 0.0001	0.046 ± 0.002	92.3 ± 2.8	69.6 ± 2.1

Notes: Error = 1 σ. * = age is the $^{206}Pb/^{238}U$ age corrected for common Pb from the measured $^{207}Pb/^{206}Pb$. † = outlier excluded from age calculation.

Table T4. Apatite fission track analytical results.

Hole, core	Lithology	Number of grains	Standard track density (× 10^6/cm²)	Fossil track density (× 10^4/cm²)	Induced track density (× 10^5/cm²)	χ^2 probability (%)	Central age ±1 σ (Ma)	Mean track length* (µm)	Standard deviation (µm)
180-1108B-6R	Microgranite clast	22	1.43 (4919)	4.97 (27)	4.652 (2527)	25	2.8 ± 0.6	14.6 ± 0.4 (5)	1.0

Notes: Parentheses enclose number of tracks counted (density) or measured (track length). Standard and induced track densities were measured on mica external detectors (geometry factor = 0.5), and fossil track densities were measured on internal mineral surfaces. Apatites were mounted in epoxy resin on glass slides, ground and polished to reveal an internal surface, and then etched for 20 s at room temperature in 5-N HNO_3 to reveal spontaneous fission tracks. Apatite ages were determined using the external detector method. Samples were irradiated at the Oregon State University Nuclear reactor in the slow soaker position B-3 (thermal column number 5), which has a Cd for Au ratio of 13.6 at the column face. The mounts were counted at a magnification of 1250×. Ages were calculated using the zeta calibration method (zeta = 361 ± 10 for dosimeter glass CN5) following the procedures of Hurford and Green (1983) and Green (1985). Analytical errors were calculated using the "conventional method" (Green, 1981). The χ^2 test performed on single-grain data (Galbraith, 1981) determines the probability that the counted grains belong to a single age population (within Poissonian variation). If $\chi^2 < 5$%, it is likely that the grains counted represent a mixed-age population with real age differences between single grains. Track lengths were measured using "confined" fossil fission tracks using only those that were horizontal (Laslett et al., 1984). Tracks were measured under a 100× dry objective using a projection tube and a digitizing tablet attached to a microcomputer.

CHAPTER NOTE*

N1. 19 February 2002—Robertson, A.H.F., Awadallah, S., Gerbaudo, S., Lackschewitz, K.S., Monteleone, B., Sharp, T.R., and other members of the Shipboard Scientific Party, 2001. Evolution of the Miocene–Recent Woodlark rift basin, SW Pacific, inferred from sediments drilled during Ocean Drilling Program Leg 180. *In* Wilson, R.C.L., Whitmarsh, R.B., Taylor, B., and Froitzheim, N. (Eds.), *Non-Volcanic Rifting of Continental Margins: A Comparison of Evidence from Land and Sea,* Spec. Publ.—Geol. Soc. London, 187:335–372.

*Dates reflect file corrections or revisions.